PLOS Computational Biology

RESEARCH ARTICLE

Closed-loop real-virtual interactions validate 3D model of social coordination in fish

Ramón Escobedo[1,2,3,4], **Justine Reynaud**[1], **Renaud Bastien**[1], **Stéphane Sanchez**[3], **Clément Sire**[2], **Guy Theraulaz**[1]*

1 Centre de Recherches sur la Cognition Animale, Centre de Biologie Intégrative, CNRS, Université de Toulouse III – Paul Sabatier, Toulouse, France, **2** Laboratoire de Physique Théorique, CNRS, Université de Toulouse III – Paul Sabatier, Toulouse, France, **3** Institut de Recherche en Informatique de Toulouse (IRIT), Université Toulouse Capitole, Toulouse, France, **4** Departamento de Matemáticas, Universidad Carlos III de Madrid, Leganés, Madrid, Spain

* guy.theraulaz@univ-tlse3.fr

OPEN ACCESS

Citation: Escobedo R, Reynaud J, Bastien R, Sanchez S, Sire C, Theraulaz G (2026) Closed-loop real-virtual interactions validate 3D model of social coordination in fish. PLoS Comput Biol 22(8): e1014544. https://doi.org/10.1371/journal.pcbi.1014544

Editor: Nir Gov, Weizmann Institute of Science, ISRAEL

Received: March 12, 2026

Accepted: July 8, 2026

Published: August 3, 2026

Peer Review History: PLOS recognizes the benefits of transparency in the peer review process; therefore, we enable the publication of all of the content of peer review and author responses alongside final, published articles. The editorial history of this article is available here: https://doi.org/10.1371/journal.pcbi.1014544

Abstract

Collective motion in animal groups arises from social interaction rules, yet uncovering these rules requires quantitative models grounded in real behavior. We developed a fully three-dimensional, data-driven model of pairwise interactions in the schooling fish *Hemigrammus rhodostomus*, reconstructing the attraction and alignment interactions from experiments with two real fish swimming freely in a hemispherical bowl. Simulations of this model quantitatively reproduced empirical distributions of speed, distance, and orientation. We then embedded the model into a closed-loop virtual reality system, allowing a real fish to interact in real time with a virtual conspecific whose movements were governed by the same interaction rules. This biohybrid setup revealed that the model captures key social interactions underlying coordinated swimming. Our results establish a robust validation framework linking data, models, and behavior, paving the way for hybrid biological-digital collectives.

Author summary

Which social interactions allow animal groups to coordinate their movements in a collective and coherent way? This question lies at the heart of research on collective behavior. In our study, we focus on small schooling fish and examine whether the rules governing their behavior can be identified and whether they are sufficient to explain how they interact. To address this, we combined detailed behavioral measurements with a virtual reality system. We first reconstructed how pairs of real fish adjust their speed and swimming direction in response to one another and to their environment. We then used these rules to build a three-dimensional model of fish motion. Crucially, we went one step further by embedding this model back into the real world. A live fish was allowed to interact in real time with a virtual partner controlled by the model. We found that real

Data availability statement: The datasets generated during and/or analyzed during the current study are available at: 10.6084/m9.figshare.30539666.

Funding: This work was funded by Agence Nationale de la Recherche (https://anr.fr/) under grant ANR-20-CE45-0006 (including salary to R.E., R.B., and non-salary costs). R.E. was also partially supported by Agencia Estatal de Investigación (https://www.aei.gob.es/) under grant PID2020-115088RB-I00. The funders had no role in study design, data collection and analysis, decision to publish, or preparation of the manuscript.

Competing interests: The authors have declared that no competing interests exist.

fish readily coordinate with this virtual partner, showing that our model captures key features of their social behavior. At the same time, small mismatches revealed the importance of factors such as speed and responsiveness. Overall, our approach provides a powerful way to test behavioral models and opens new possibilities for studying hybrid systems in which real and virtual agents interact.

1 Introduction

Collective motion in animal groups is an archetype of distributed coordination. Fish schools, bird flocks, and insect swarms turn, accelerate, and reconfigure without central control, suggesting that local interaction rules can generate coherent global patterns [1]. The central question is how to identify those interaction rules and test whether they are able to reproduce the observed coordination in realistic settings [2]. Decades of work show that collective motion can emerge from simple alignment, attraction, and repulsion rules, modulated by noise and density. Models of self-propelled particles reproduce transitions between disorder and ordered motion and recover milling, swarming, and polarized states when parameters vary in plausible ranges [1,2]. At the same time, empirical studies emphasize biological specificity. Individuals differ in responsiveness, perception is anisotropic, and boundaries shape trajectories. These factors complicate the mapping from model rules to measured behavior [3,4]. Fish, in particular, offer a tractable system to bridge models and data. High-resolution tracking allows reconstruction of how burst-and-coast swimmers turn in response to neighbors and walls, revealing distinct alignment and attraction components that vary with distance, bearing, and relative heading. Previous work has shown that such behavioral analyses provide a solid foundation for constructing realistic models of schooling dynamics [5–7].

Virtual reality (VR) closes this loop by embedding animals in responsive, programmable environments [8–10]. Immersive systems for freely moving animals project visual stimuli that update in real time with the subject's motion, enabling experiments with high ecological validity and precise control over sensory input [11–13]. In fish, VR has been used to probe neural and behavioral mechanisms of social perception and prediction (Fig 1A). Adult zebrafish in head-fixed VR exhibit robust, naturalistic behaviors, while neural imaging reveals circuits sensitive to prediction error when expected visual flow mismatches actual sensory input [14,15]. Recent work also reverse-engineers pursuit and schooling control laws using closed-loop VR, showing that simple proportional-derivative rules on egocentric distance can explain target tracking across contexts [16]. VR studies further show that reciprocal interactions are necessary for natural temporal coordination, which emerges as an alternating rhythm of bursts that enhances spatial responsiveness [17].

Despite this progress, a key gap remains. Most validations of collective-behavior models rely on statistical similarity between simulated and experimental distributions (see for instance [5–7]). Agreement in speed, spacing, or turning statistics is necessary, but not sufficient, to demonstrate that a model encodes the causal social

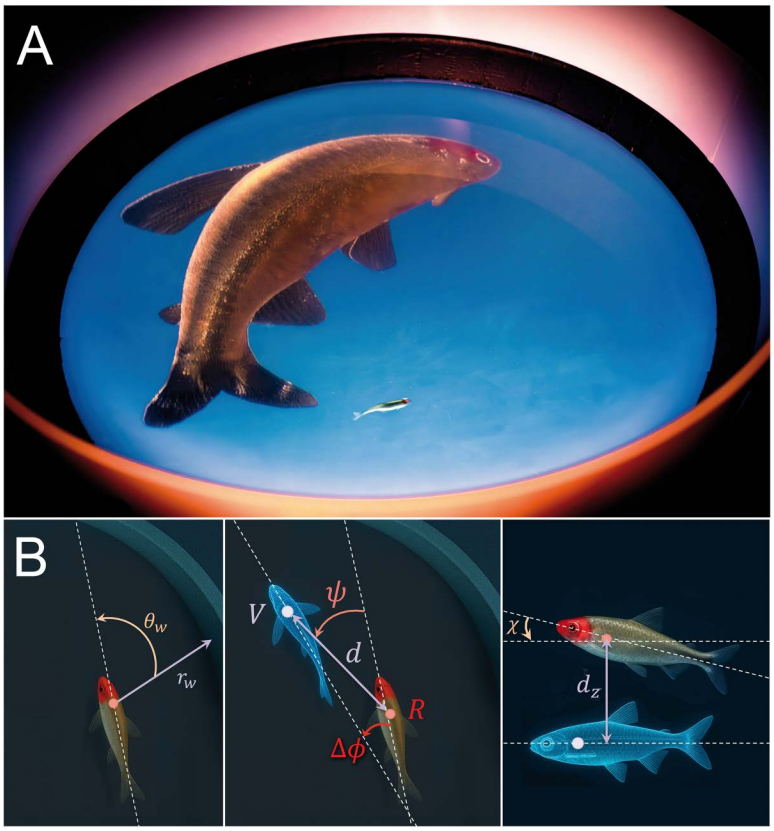

Fig 1. Closed-loop 3D virtual reality system and interaction geometry. (A) In the virtual reality setup, the 3D movements of a freely swimming fish are tracked in real time to feed a mathematical model of a virtual conspecific whose 3D anamorphic image is projected onto the inner surface of the hemispherical tank, allowing the model to continuously update the virtual fish's position and orientation based on the real fish's movements (Photo by David Villa, ScienceImage/CBI/CNRS, Toulouse). **(B)** Variables used to describe the distance r_w and relative orientation of the real fish to the wall θ_w (left); the distance d, viewing angle ψ and relative orientation $\Delta\phi$ of the real fish with respect to the virtual fish (middle), and the vertical angle of the real fish χ and the vertical distance between fish d_z (right).

https://doi.org/10.1371/journal.pcbi.1014544.g001

interactions used by real animals. The stronger test is behavioral and consists in embedding a model-controlled agent into the interaction loop and asking whether a real conspecific responds as it would to a live partner. This test becomes more demanding in 3D, where vertical dynamics, wall effects, and the geometry of perception combine to shape motion. It also requires models that integrate individual self-propulsion, boundary interactions, and social responses into a single, data-driven framework.

Our study addresses this challenge in three steps, focusing on *Hemigrammus rhodostomus*, a small tropical freshwater species that exhibits remarkably cohesive schooling behavior and has become a model organism for studying the mechanisms underlying collective motion [5,6,18–21]. First, we quantify the interaction functions between two real fish swimming freely in a semi-spherical bowl. We reconstruct how horizontal acceleration decomposes into parallel and perpendicular components relative to heading, and how these components vary with velocity, neighbor distance, relative position, and heading difference, as well as with wall distance and incidence angle. We also characterize the vertical dynamics through vertical friction, preferred depth, and vertical attraction to a common depth. This reconstruction follows a data-driven approach that has proven effective in planar setups, extended here to full 3D kinematics [22]. Second, we build a 3D

self-propelled particle model that embeds those reconstructed functions, together with stochastic terms extracted from the data. We then test the model by comparing simulations of two virtual agents to experimental baselines of two real fish, assessing agreement across individual and collective observables. Third, we integrate the validated model into an immersive VR system [23]. The anamorphic image of a digital twin of a fish is projected onto the inner surface of the bowl and controlled in real time by the model, using the tracked position and heading of the live fish as input (Fig 1A). This hybrid setup lets us test whether the same interaction functions that reproduce real–real pairs in silico can also elicit natural coordination when one partner is virtual.

This pipeline enables three scientific questions. First, can interaction functions inferred from real–real pairs replicate individual and pair-level behavior in 3D simulations? Second, when one agent is virtual and controlled by the same model, does a real fish coordinate with it as with a real conspecific, and how do any deviations illuminate missing mechanisms such as actuation limits or latency? Third, how do the virtual partner's speed and reciprocity modulate coordination strength, spacing, and alignment? Speed is a key control parameter for cohesion and polarization in fish groups, with faster kinematics often enhancing alignment and reducing reaction delays in both fish and birds [24–26]. Reciprocity also matters: theory and experiments show that influence and leadership in moving groups depend on mutual responsiveness and timing [27,28]. We designed the closed-loop experiments to probe these mechanisms directly.

This approach complements neural and control-law studies in VR with zebrafish by focusing on full-body 3D kinematics in freely swimming social fish and by combining model reconstruction, forward simulation, and closed-loop behavioral validation in a single experimental framework [14–16]. It also builds on the demonstration that visual cues alone can sustain coordinated motion in social fish and that immersive VR can evoke ecologically meaningful responses in freely moving species [12,29–33]. Previous studies have demonstrated that visual cues alone can sustain social responses in fish and that biological motion plays a key role in triggering affiliation. In particular, zebrafish have been shown to robustly shoal with simple visual stimuli reproducing fish-like motion kinetics, even in the absence of reciprocal interaction [34]. At the same time, control experiments using non-social moving objects have revealed that not all motion cues are equally effective. In a recent study using a similar virtual reality setup, fish did not follow or coordinate well with a simple moving sphere lacking biologically realistic motion or interaction dynamics, highlighting the specificity of social responses to appropriate visual and kinematic features [23]. These findings underline the importance of identifying which aspects of motion and interaction are necessary to elicit coordinated behavior. By placing a digital twin into a natural feedback loop, we move beyond validation at the level of static distributions and test directly whether the inferred social interactions produce the expected behavioral responses.

In sum, we address a core challenge in collective behavior and move from models that fit statistics to models that pass behavioral tests in closed loop. This hybrid strategy advances the validation of interaction rules in living systems and opens a path toward mixed collectives where biological and digital agents coordinate under shared rules.

2 Results

2.1 Quantitative analysis of pairwise swimming dynamics

Fig 1B illustrates the main kinematic and geometric quantities used throughout this study to characterize and quantify fish motion, as well as the influence of social interactions on it. A detailed definition and mathematical description of these variables are provided in the Materials and Methods section.

Fig 2 shows the experimental distributions obtained from two real fish, together with their counterparts from numerical simulations of the model described below, for a set of key descriptors of individual and collective motion. The probability density functions of the full 3D speed v^{3D} and inter-individual 3D distance d^{3D} are nearly indistinguishable from those of their horizontal projections v and d, respectively (see S1 Fig), indicating that motion remains mostly planar. While this result reflects the strong tendency of fish to align vertically in pairwise interactions, it does not preclude the emergence of

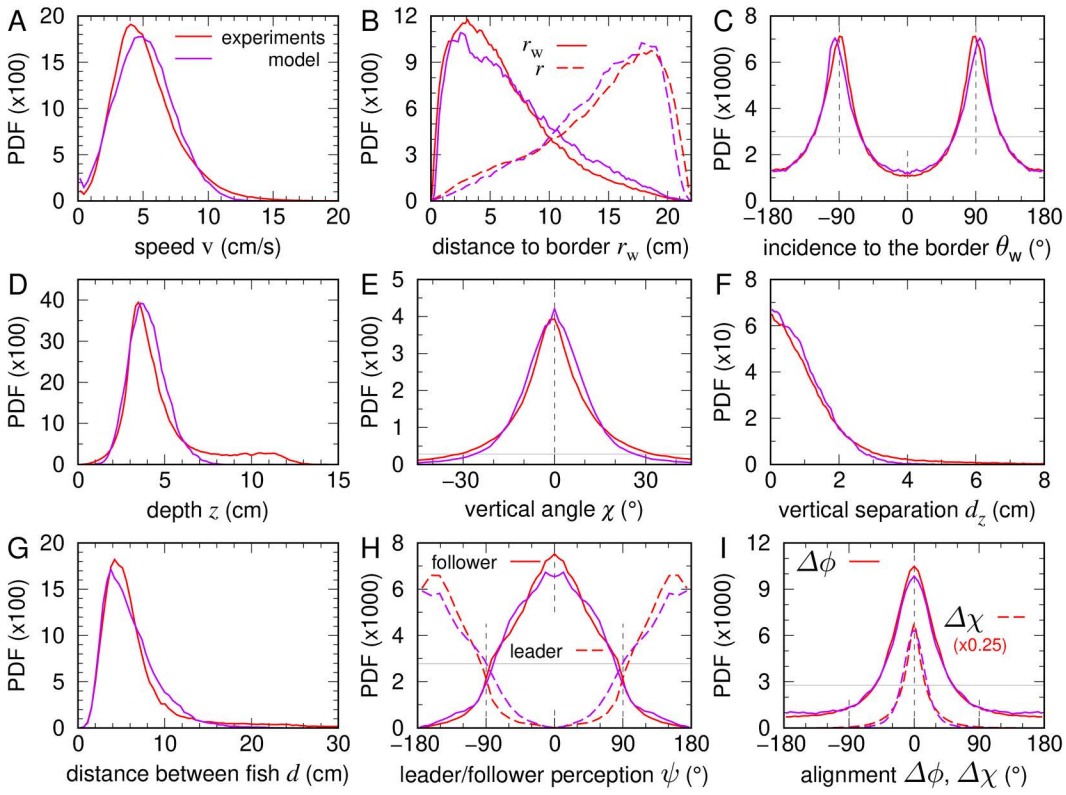

Fig 2. Quantification of free swimming behavior in a fish pair within the hemispherical bowl. Probability density functions (PDFs) of (A) swimming speed v, (B) distance to the bowl wall r_w (solid lines) and radial position r (dashed lines), (C) incidence angle relative to the wall θ_w, (D) swimming depth z, (E) elevation angle χ, (F) vertical inter-individual distance d_z, (G) horizontal inter-individual distance d, (H) viewing angle of the neighbor ψ when acting as the geometrical follower (solid lines) or geometrical leader (dashed lines), and (I) heading misalignment in the horizontal plane $\Delta\phi$ (solid lines) and vertical plane $\Delta\chi$ (dashed lines). Red curves represent experimental data from two real fish, whereas purple curves correspond to numerical simulations of the model. Horizontal gray lines in (C, E, H, I) indicate the uniform angle distribution value, 1/360 ($\approx 2.78 \times 10^{-3}$).

https://doi.org/10.1371/journal.pcbi.1014544.g002

three-dimensional structure in larger groups, where interactions with multiple neighbors may lead to more complex spatial organization [35].

Fish swam at a preferred speed of approximately $v \approx 5$ cm/s (Fig 2A), rarely exceeding 10 cm/s. Note that this speed range is markedly lower than observed in quasi-2D experiments in shallow water [5], where the mean speed was close to 10 cm/s, which might be ascribed to lower light levels in the VR experimental setup. The fish remained close to the wall of the bowl, with a mean wall distance $r_w \approx 3$ cm (Fig 2B), corresponding to a radial position $r \approx 18$ cm from the central vertical axis. Their heading angle relative to the wall, θ_w, was concentrated slightly below 90° (Fig 2C), indicating motion nearly tangential to the boundary. The fish also exhibited a preferred swimming depth around $z \approx 4$ cm (Fig 2D), with occasional excursions toward the bottom (uniform tail over $z \in [7, 12]$ cm, with maxima up to 13 cm). Vertical motion was minimal overall: the elevation angle χ remained tightly centered around zero (Fig 2E), confirming the strong preference for horizontal navigation.

At the collective level, individuals stayed in close proximity, with a typical horizontal separation $d \approx 5$ cm (Fig 2G) and a very small vertical separation $d_z < 2$ cm (Figs 2F and S1). As shown in Fig 2H, a clear leader–follower configuration emerged: the follower typically viewed the leader directly ahead (solid curves peaked near zero), whereas the leader perceived the follower behind, with peaks near $\pm 160°$ (dashed curves). Alignment was strong in both planes, as evidenced

by the peaked distributions of heading differences $\Delta\phi$ and $\Delta\chi$ around zero (Fig 2I), the latter being particularly narrow due to minimal vertical excursions.

Another notable behavior of the fish is their spontaneous tendency to perform U-turns while swimming side by side. One fish suddenly turns around to swim in the opposite direction of its companion, which in turn performs a U-turn to rejoin the first. S3 Fig shows the probability density function (PDF) and the survival curve of the time intervals separating two successive U-turns, displaying an exponential decay.

2.2 Data-driven 3D model of pairwise coordination in fish

Building on our empirical results and extending previous 2D modeling frameworks [5–7,36], we develop a fully data-driven 3D dynamical model that accounts for the geometry of the hemispherical bowl and the social interactions underlying coordinated motion. Because of the limited precision of the three-dimensional tracking (especially along the vertical axis), segmentation of fish trajectories into discrete burst-and-coast phases was not feasible. As a consequence, we could not rely on the burst-and-coast–type description and model previously developed in two dimensions [5]. It was therefore necessary to modify the model structure and adopt a continuous-time formulation of fish motion.

The instantaneous behavioral state of a fish is represented by the 9 variables v, v_z, r_w, θ_w, z, d, d_z, ψ, $\Delta\phi$, respectively describing its horizontal and vertical speed, its distance and orientation with respect to the wall, its depth relative to the water surface, and its horizontal and vertical distance, viewing angle, and heading relative to another fish (see Fig 1B). The temporal evolution of these variables combines biomechanical constraints, interactions with the environment, and social cues from the neighbor. The associated equations of motion are based on principles of self-organization, symmetry, and collision avoidance, and their functional forms are quantitatively inferred from the experimental data using a reconstruction procedure generalized from flat-arena studies to a curved 3D geometry [5]. A detailed description of the model is provided in Materials and Methods.

We decompose fish motion into horizontal and vertical components:

$$\frac{d\vec{v}(t)}{dt} = -\vec{F}_\mathrm{water}(\vec{v}) - \vec{F}_\mathrm{adapt}(\vec{v}) - \vec{F}_\mathrm{w}(r_\mathrm{w},\theta_\mathrm{w}) + \vec{F}_\mathrm{rot}(r_\mathrm{w},\theta_\mathrm{w}) + \vec{F}_\mathrm{Att}(d,\psi,\Delta\phi) + \vec{F}_\mathrm{Ali}(d,\psi,\Delta\phi) + \vec{\eta}, \tag{1}$$

$$\frac{d\mathrm{v}_z(t)}{dt} = -F^z_\mathrm{water}(\mathrm{v}_z) - F^z_\mathrm{comfort}(z) + F^z_\mathrm{Att}(d,d_z,\psi,\Delta\phi) + \eta_z. \tag{2}$$

In the horizontal plane, the acceleration $\vec{a}(t) = d\vec{v}(t)/dt$ results from six forces: **(i)** an effective friction emerging from hydrodynamic effects and the tendency of fish to swim at a preferred speed, $-\vec{F}_\mathrm{water}$, **(ii)** a term implementing the tendency of a fish to adapt its speed to that of its neighbor (or to the average speed $\bar{\mathrm{v}}$ of its neighbors for more than one neighbor), of magnitude $F_\mathrm{adapt}(\vec{v}) = f_\mathrm{adapt}(\mathrm{v}-\bar{\mathrm{v}})$, **(iii)** a radial repulsive interaction with the wall of the bowl, $-\vec{F}_\mathrm{w}$, **(iv)** a wall-induced rotational force guiding motion tangentially, $\vec{F}_\mathrm{rot}$, and **(v-vi)** the social attraction and alignment interactions with the neighbor, $\vec{F}_\mathrm{Att}$ and $\vec{F}_\mathrm{Ali}$. In the vertical direction, $a_z(t) = d\mathrm{v}_z(t)/dt$ arises from **(i)** a friction acting on the vertical speed $-F^z_\mathrm{water}$, encapsulating the tendency of a fish to swim horizontally, **(ii)** a tendency to swim at a preferred comfort depth, $-F^z_\mathrm{comfort}$, which also effectively results from the interaction of the fish with the wall of the bowl and the surface of the water, and **(iii)** a vertical attraction toward the neighbor's depth, F^z_Att. Additionally, a noise term is added to each component, $\vec{\eta}$ and η_z respectively, corresponding to the fish spontaneous decisions and random changes of heading.

A powerful assumption of our modeling process consists in considering that, once decomposed along the parallel and perpendicular components of the acceleration, the magnitudes of the forces are separable as products of single-variable functions, e.g., $F_\mathrm{w}(r_\mathrm{w},\theta_\mathrm{w}) = f_\mathrm{w}(r_\mathrm{w})g_\mathrm{w}(\theta_\mathrm{w})$. Moreover, symmetry constraints apply to the angular functions to consistently reproduce the directional reactions of fish. For instance, the rotational force $F_\mathrm{rot}(r_\mathrm{w},\theta_\mathrm{w})$ must be an odd function of θ_w at fixed r_w (hence, including a factor $\sin(\theta_\mathrm{w})$) ensuring that a fish approaching the wall with $\theta_\mathrm{w} > 0$ (wall to its right) would

turn in the opposite direction to that taken if it were approaching the wall with the opposite angle $-\theta_w < 0$. This constraint preserves the right-left symmetry, which was shown to consistently hold for the considered fish species [5]. Similarly, the alignment force $F_{Ali}(d, \psi, \Delta\phi)$ must include a factor $\sin(\Delta\phi)$ favoring a left turn when the neighbor is oriented counter-clockwise with respect to the heading of the focal fish ($\Delta\phi > 0$) by increasing the perpendicular acceleration, while if the neighbor is oriented relatively clockwise ($\Delta\phi < 0$), the negative contribution induces a right turn.

Thus, with these separability and symmetry considerations, the magnitudes of the forces induced by the wall are given by

$$F_w(r_w, \theta_w) = f_w(r_w)\, g_w(\theta_w), \tag{3}$$

$$F_{rot}(r_w, \theta_w) = f_{rot}(r_w)\, g_{rot}(\theta_w) \sin(\theta_w), \tag{4}$$

where $g_w(\theta_w)$ and $g_{rot}(\theta_w)$ are even functions of θ_w. As for the social interactions, they can be written as

$$F_{Att}(d, \psi, \Delta\phi) = f_{Att}(d)\, g_{Att}(\psi)\, h_{Att}(\Delta\phi), \tag{5}$$

$$F_{Ali}(d, \psi, \Delta\phi) = f_{Ali}(d)\, g_{Ali}(\psi)\, h_{Ali}(\Delta\phi) \sin(\Delta\phi), \tag{6}$$

$$F^z_{Att}(d, d_z, \psi, \Delta\phi) = f^z_{Att}(d)\, k^z_{Att}(d_z)\, g^z_{Att}(\psi)\, h^z_{Att}(\Delta\phi), \tag{7}$$

where all g and h functions of an angle are even. These interactions involve interaction functions depending on the distance between the fish and its neighbor or the wall, which are modulated by angular functions effectively describing the fish anisotropic perception of its environment.

The model also includes simple rejection rules that prevent the fish from crossing the physical wall of the bowl or the water surface. When a predicted step places the fish beyond these boundaries, the movement is rejected and a new fish orientation or vertical movement is recalculated (see Material and Methods for more details).

The resulting stochastic differential system is solved numerically using the Euler–Maruyama scheme with experimentally informed initial conditions.

2.3 Reconstruction of empirical interaction functions and validation of the 3D behavioral model

In this section, we present the interaction functions empirically reconstructed from the experimental trajectories and analyze their biological and dynamical roles in shaping coordinated motion. This method was originally introduced in [5] and extended in [22] and was extensively exploited to analyze the interactions arising from effectively 2D burst-and-coast trajectories, relevant to the case of fish swimming in shallow water. Here, we simply extend the method to 3D trajectories and to a continuous-time formulation of the equations of motion.

The general idea of the method consists in describing the different single-variable interaction functions introduced in the previous section by polynomial expansions, Fourier series, or tabulations. Ultimately, the parameters involved in this description are optimized to minimize the discrepancy between the observed acceleration of a real fish and the acceleration predicted by the model.

Some of the functions introduced above have a general shape that can be guessed on physical principles. For instance, the magnitudes (denoted with lowercase f) of the friction terms and the speed adaptation term are expected to resemble the following functional forms:

$$f_{water}(v) \approx \frac{v - v_0}{\tau_0}, \quad f^z_{water}(v_z) \approx \frac{v_z}{\tau_z}, \quad f_{adapt}(v - \bar{v}) \approx \frac{v - \bar{v}}{\tau_{adapt}}. \tag{8}$$

The friction $f_{\text{water}}(v)$ tends to maintain a speed v_0 over a relaxation time τ_0, while $f^z_{\text{water}}(v_z)$ ensures that the mean vertical speed in a bounded bowl must necessarily be zero (i.e., that the fish is on average aligned with the horizontal plane). Finally, $f_{\text{adapt}}(v-\bar{v})$ enforces the tendency of a fish to match its speed v to the speed $\bar{v}$ of its neighbor(s). In our reconstruction procedure, we are not imposing these simple but natural linear forms, and the functions are instead expanded as a finite order polynomial of their variable (in practice, we used third-order polynomials; see for instance, Eqs. (S1), (S2), and (S12) in Supplemental Material). Similarly, some interaction functions are expected to vanish linearly for some value of their corresponding variable and will also be described by finite-order polynomials. This is the case for $k^z_{\text{Att}}(d_z)$ (expected to vanish at a vertical separation between fish $d_z = 0$) and $f^z_{\text{comfort}}(z)$ (expected to vanish at some preferred depth $z = z_0$). Hence, in total, 5 functions are described as polynomials of their corresponding variable, whose coefficients are to be optimized by the reconstruction procedure.

Moreover, the model involves 8 angular functions (depending on the angles θ_w, ψ, or $\Delta\phi$) modulating the magnitude of the interaction of a fish with the wall and its attraction/alignment to its neighbor(s), and encoding the fish's anisotropic perception of its environment. These angular functions are expressed as even Fourier series (preserving the left-right symmetry closely maintained by the considered fish [5]) of the form $1 + \sum_{k=1}^{K} c_k \cos(kx)$, where the c_k's are parameters to be optimized. We allowed up to $K = 6$ Fourier modes for each function, although for 2D trajectories, 2 or 3 modes were found to be sufficient to capture the different interaction functions [5].

Finally, for the 5 interaction functions $f_w(r_w)$, $f_{\text{rot}}(r_w)$, $f_{\text{Att}}(d)$, $f_{\text{Ali}}(d)$, and $f^z_{\text{Att}}(d)$, no general insight on their shape can be ascertained from physical/biological considerations. Hence, following [5,22], we tabulate each of them over a finite grid (typically, 0.5 cm spacing for the grids for r_w and d) of their corresponding variable and consider the value of the function at each point of the grid as a parameter to be optimized. After optimization, the resulting functions are fitted by simple functional forms, which are ultimately implemented in the model. These fitting functions and the different polynomial and Fourier expansions introduced above are detailed in the Supplemental Material.

The coefficients of the 5 polynomial expansions, those of the 8 Fourier series, and the parameters of the 5 tabulated functions are then optimized by minimizing the error between the experimentally measured accelerations and those predicted by the model. We use the total squared error $\Delta = \Delta_{\parallel} + \Delta_{\perp} + \Delta_z$, where each term measures the squared difference between the experimental and model components of the acceleration along the fish heading, perpendicular to it, and along the vertical axis, $a_{\parallel}$, $a_{\perp}$, and a_z, respectively (the detailed forms of $a_{\parallel}$, $a_{\perp}$, and a_z in the model are given in Materials and Methods). The matching error along the three directions are thus

$$\Delta_{\xi} = \sum_{\text{data}} \left(a_{\xi}^{\text{exp}} - a_{\xi}^{\text{model}} \right)^2 ,$$

for $\xi = \parallel$, $\perp$, and z, and where each model acceleration is evaluated using the values of $(v, v_z, r_w, \theta_w, z, d, d_z, \psi, \Delta\phi)$ observed in the corresponding experimental data.

Experimental accelerations are computed by finite differences after a slight smoothing of the experimental trajectories (see Materials and Methods). The model accelerations depend on the unknown functions introduced above. The coefficients describing their polynomial or Fourier expansion, or their tabulation parameters, are therefore the unknowns of the minimization problem. Because each force contributes linearly to the acceleration due to the separability assumption, Δ is quadratic with respect to the tabulated function values, thus allowing the efficient use of a gradient-descent optimization scheme to minimize the matching error Δ.

Fig 3 depicts the reconstructed functions (colored curves) superimposed on the PDF of their corresponding variable (gray areas). This highlights the regions of highest data density, where the reconstruction is most reliable and which primarily determine the overall shape of the functions.

The horizontal drag $f_{\text{water}}(v)$ reduces speeds greater than $v \approx 3.5$ cm/s, and increases speeds below it (Fig 3A). The speed adaptation function $f_{\text{adapt}}(v-\bar{v})$ is essentially linear in the difference between the speed of a focal fish and that of its neighbor, as anticipated above (see Eq. (8)).

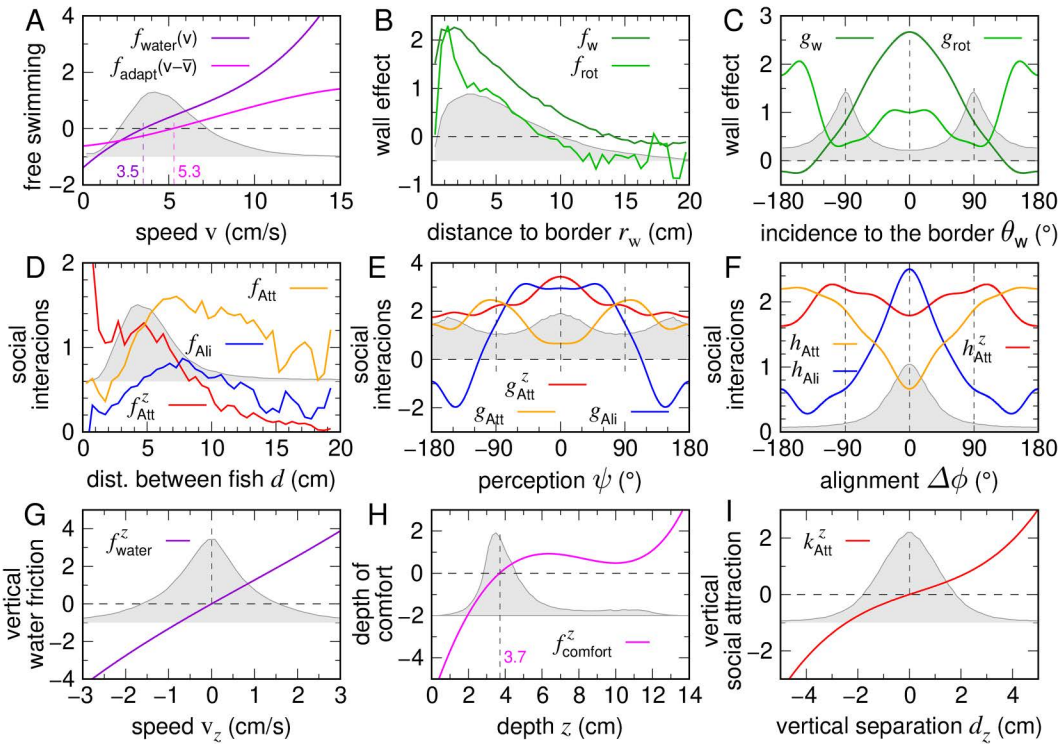

Fig 3. Experimentally reconstructed locomotion and interaction functions. Colored solid curves: reconstructed force components inferred from the experimental data. Gray areas: corresponding probability density functions (PDFs) of the associated state variables. **(A)** Self-propulsion terms: hydrodynamic friction and relaxation toward a preferred speed, $f_{water}(v)$ and tendency of a fish to adapt its speed to that of its neighbor, $f_{adapt}(v-\bar{v})$ (arbitrarily centered at $\bar{v}$ equal to the mean speed in this plot) as functions of the horizontal speed v. **(B)** Interaction with the wall: radial repulsion $f_w(r_w)$ and wall-induced rotation $f_{rot}(r_w)$ as functions of the distance to the wall r_w. **(C)** Angular modulation of wall effects through $g_w(\theta_w)$ and $g_{rot}(\theta_w)$ as functions of the incidence angle θ_w. **(D)** Social interactions as functions of the horizontal distance between individuals d: horizontal attraction $f_{Att}(d)$, vertical attraction $f^z_{Att}(d)$, and horizontal alignment $f_{Ali}(d)$. **(E, F)** Angular modulation of the social interactions as functions of the viewing angle ψ and heading difference $\Delta\phi$. **(G)** Vertical drag $f^z_{water}(v_z)$ as a function of vertical speed v_z. **(H)** Attraction toward a preferred depth $z_0 \approx 3.7$ cm, $f^z_{comfort}(z)$, as a function of the depth z. **(I)** Vertical attraction between fish $k^z_{Att}(d_z)$ as a function of the vertical separation between fish d_z. In these plots, the angular functions have been normalized such that $\int_{-\pi}^{\pi} g^2(x)\,dx = \int_{-\pi}^{\pi} h^2(x)\,dx = 2\pi$.

https://doi.org/10.1371/journal.pcbi.1014544.g003

The wall-repulsion function $f_w(r_w)$ is strong when the fish is within 6 cm of the wall (i.e., about 2 body lengths, consistent with the results of [5] for quasi-2D experimental setups) and essentially vanishes for $r_w \gtrsim 13$ cm (see Fig 3B). The wall-induced rotational component $f_{rot}(r_w)$ has a similar spatial profile but a weaker magnitude. Both are modulated by even angular functions (see Fig 3C) encapsulating the fish's anisotropic perception of the wall, with the modulation of the repulsion to the wall $g_w(\theta_w)$ peaking at $\theta_w = 0$, when the fish is facing the wall, and being suppressed by a factor of 2 or more for $|\theta_w| > 90°$.

The horizontal attraction and alignment interactions $f_{Att}(d)$ and $f_{Ali}(d)$ initially grow with the distance between fish and then peak at $d \approx 2$–3 body lengths (7–9 cm), before slowly decaying for $d \gtrsim 12$ cm, although the reliability of this long-range behavior is poor due to a lack of observed data, as fish are rarely found at such distances (Fig 3D). The vertical attraction $f^z_{Att}(d)$ extends over a slightly narrower range.

Angular modulations reveal that social attraction is stronger when the neighbor is located laterally (maxima of g_{Att} near $\psi = \pm 90°$, Fig 3E), and more pronounced as the fish become more misaligned, with h_{Att} increasing as $|\Delta\phi|$ goes from 0 to 180° (Fig 3F). Alignment is stronger when the neighbor is in front ($|\psi| < 60°$, Fig 3E) and becomes anti-alignment when the neighbor is behind ($g_{Ali} < 0$ when $|\psi| > 120°$). Furthermore, alignment weakens as the fish are more misaligned

(h_{Ali} decreases as $|\Delta\phi|$ goes from 0 to 180°; see Fig 3F). This apparent anti-alignment should not be interpreted as an attraction-like response. Instead, it results from the angular dependence of the alignment interaction (Fig 3E), which promotes turning when a neighbor is located behind the focal fish, independently of their relative orientation.

As anticipated above (see Eq. (8)), the vertical friction $f^z_{\mathrm{water}}(v_z)$ is a nearly linear odd function that suppresses vertical excursions (see Fig 3G). The effective force $f^z_{\mathrm{comfort}}(z)$ driving the fish toward a preferred depth $z_0 \approx 3.7$ cm (see Fig 3H) exhibits a stronger/steeper repulsive interaction with the surface of the water ($z=0$) than with the bottom of the bowl. For the interaction between fish along the vertical direction, the observed modulation by ψ and $\Delta\phi$ is weak, indicating that vertical attraction depends primarily on the depth difference (the weakly nonlinear and almost odd $k^z_{\mathrm{Att}}(d_z)$ in Fig 3I) and on the distance between fish ($f^z_{\mathrm{Att}}(d)$ in Fig 3D, which is strongly suppressed for $d>10$ cm).

Fig 2 shows that the agreement between experimental data and simulations of the model integrating the empirically reconstructed interaction functions is excellent. This agreement holds for both horizontal kinematic variables, such as speed, relative position, and heading, and vertical components, including swimming depth z and vertical orientation χ. Moreover, the model also accurately reproduces the time intervals separating two consecutive U-turns (S3 Fig).

2.4 Closed-loop experiments with a virtual conspecific controlled by the model

Having established the natural coordination patterns of two real fish and derived a data-driven model that accurately reproduces these dynamics, we next examined how a real fish behaves when it interacts with a virtual conspecific whose motion is controlled in real time by the model.

We tested three closed-loop conditions, each differing in the behavioral parameters assigned to the virtual fish, to probe the role of reciprocity and kinematics in social coordination. In preliminary observations, we found that real fish swim significantly faster in the VR setup than in real–real interactions, likely due to environmental differences such as illumination. To account for this discrepancy, we introduced conditions with different speed regimes for the virtual fish, allowing us to test whether interaction rules inferred at lower speeds generalize to higher-speed contexts:

- **Condition C1**: a perfect clone, reproducing the behavior of a real fish in a pair, swimming with a mean speed $v \approx 5$ cm/s;
- **Condition C2**: a faster clone moving at twice the speed used in condition C1 ($v \approx 10$ cm/s, similar to what is observed in quasi-2D experiments in shallow water and with a standard lighting [5]);
- **Condition C3**: a faster clone identical to the one used in condition C2 but which is independent of the real fish, creating a one-way interaction where only the real fish responds.

These closed-loop assays allow us to quantify how a real fish adjusts its behavior depending on the speed and responsiveness of the virtual partner. By comparing the resulting probability distributions of key behavioral measurements with those obtained for two real fish (Fig 4), we can evaluate both the realism of the model and the extent to which coordination mechanisms remain engaged when interaction becomes kinematically challenging or asymmetric. Remarkably, despite substantial speed differences introduced in C2 and C3, and the absence of reciprocal interaction in C3, the real fish still exhibits similar social responses (i.e., similar pairwise separation and alignment) in response to the virtual conspecific.

2.4.1 Behavioral responses of a real fish interacting with a realistic virtual partner. We refer to the condition where both fish are real as the 2R (two real) baseline. Fig 4 reports the same observables presented in Fig 2 for condition 2R, but now corresponding to condition C1, where the real fish interacts with a model-controlled virtual clone.

The probability density functions for the real fish (red), the virtual fish (blue), and simulations of two real fish (violet) allow us to directly compare (i) the behavior of a real fish when paired with a real versus a virtual partner and (ii) how the model-defined behavior changes when the real fish deviates from its natural pairwise dynamics.

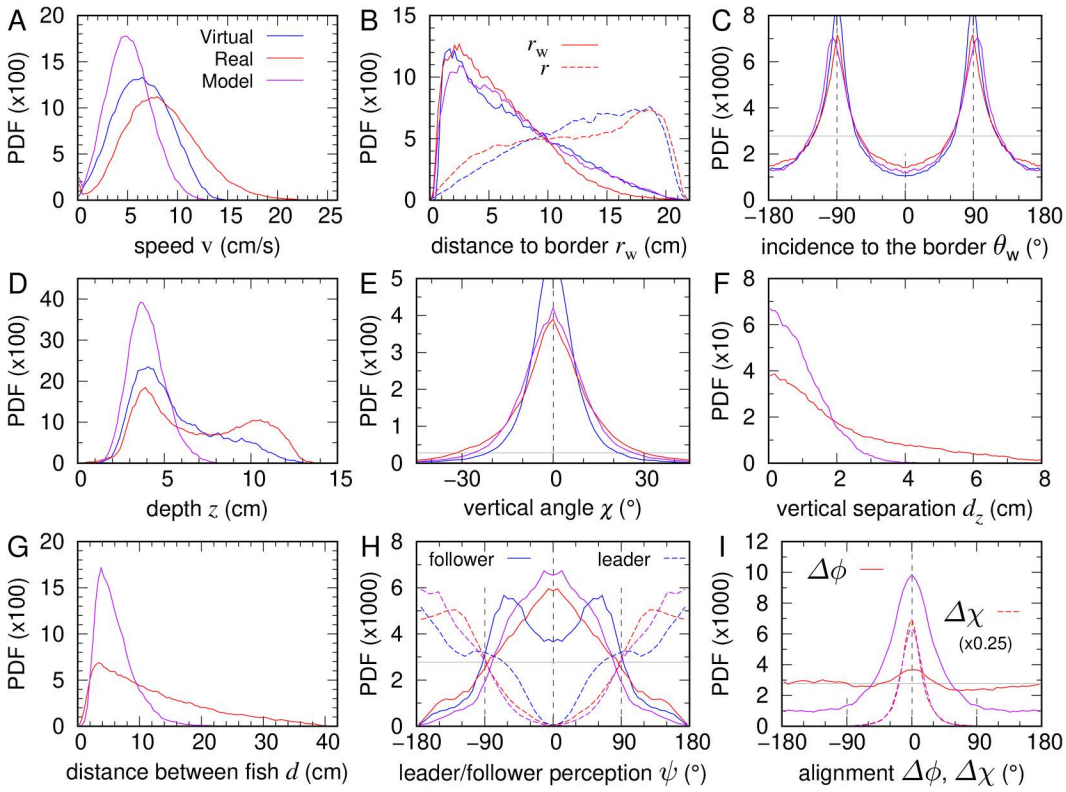

Fig 4. Model validation through real–virtual fish interactions. Probability density functions (PDFs) of behavioral variables measured for the real fish (red) interacting with a virtual conspecific controlled in closed loop by the model, for the virtual fish (blue), and for numerical simulations involving two real fish (violet). **(A)** Swimming speed v. **(B)** Distance to the wall r_w. **(C)** Incidence angle relative to the wall θ_w. **(D)** Swimming depth z. **(E)** Elevation angle χ. **(F)** Vertical inter-individual distance d_z. **(G)** Horizontal inter-individual distance ***d***. **(H)** Viewing angle ψ for geometrical leader (dashed lines) and follower (solid lines). **(I)** Heading alignment between the real and virtual fish in the horizontal plane $\Delta\phi$ (solid lines) and in the vertical direction $\Delta\chi$ (dashed lines).

https://doi.org/10.1371/journal.pcbi.1014544.g004

Overall, the qualitative features of bowl swimming remain present: real and virtual fish stay near the wall (Fig 4B), swim nearly tangentially to it (Fig 4C), maintain a preferred depth (Fig 4D), and exhibit small vertical angles (Fig 4E). Coordination is still visible, as shown in S1 Video and S2 Fig. The strong following behavior observed in these experiments relies on the perceptual realism of the projected stimulus. Because the virtual fish is rendered using a full 3D model and projected through an anamorphic transformation that accounts for the real fish's viewpoint, the stimulus is perceived as a coherent object located inside the tank. As illustrated in S1 Video, fish respond to the virtual conspecific as if it were physically present, maintaining appropriate distances and relative positioning despite the projection occurring on the curved surface of the bowl. This result highlights that the visual system of the fish integrates both geometric and kinematic cues to reconstruct a socially meaningful representation of the stimulus.

However, substantial quantitative differences emerge. Most strikingly, the real fish swims markedly faster when interacting with the virtual clone than with a real conspecific: the PDF of its speed peaks near $v \approx 8$ cm/s in C1, reaching up to 20 cm/s, whereas in 2R the speed rarely exceeds 10 cm/s (Fig 4A). In fact, the swimming speed of the real fish now aligns with the characteristic speeds documented in quasi-2D experiments [5]. As noted earlier, the projection of the virtual fish may partially restore lighting conditions comparable to those of the 2D setup, which could explain the observed agreement in swimming speeds. The virtual fish also swims faster than implemented in the model (peak near $v \approx 6.5$ cm/s instead of 5 cm/s), thanks to the speed adaptation term (see Eq. (8) and the discussion below it). However, as it is constrained by the

model's speed parameters, it cannot accelerate sufficiently to keep up with the real fish (S1 Video). This speed mismatch produces an increase in the typical distance between fish (Fig 4G) and prevents the virtual fish from positioning itself appropriately to maintain alignment (Fig 4I).

A second major difference is a more frequent bottom exploration (Fig 4D). While the real fish in 2R mostly remains near its preferred depth $z \approx 4$ cm, the real fish in C1 frequently visits the lower region of the bowl, producing a secondary PDF peak around $z \approx 10.5$ cm. The virtual clone exhibits the same trend, though less strongly.

These changes weaken spatial cohesion: the PDF of the horizontal distance between fish d broadens substantially, with $d > 20$ cm observed frequently (Fig 4G). Alignment is also drastically reduced: the PDF of $\Delta\phi$ is almost flat (Fig 4I), indicating minimal heading correlation.

The PDF of the angle of perception shows that fish still display the classic spatial configurations of geometric leader and follower. As a follower, the real fish predominantly perceives the virtual one ahead ($|\psi_{\text{follower}}| < 90°$; red solid line, Fig 4H), consistent with 2R behavior (purple line), and as leader, it perceives its neighbor behind ($|\psi_{\text{leader}}| > 90°$; red dashed line, Fig 4H). However, the virtual fish tends to perceive the real one laterally ($|\psi| \approx 60°$; blue solid line), revealing a breakdown in reciprocal leadership. As geometrical leaders, both fish maintain ψ distributions similar to real-pair interactions. The virtual fish's behavior differs subtly from that of the real one. As leader, its behavior remains similar to that observed in interactions between real fish (blue dashed line, Fig 4H). However, as a follower, it clearly keeps the real fish in front but at one side, as shown by the two peaks of the PDF of ψ_{follower} at $\pm 60°$ (blue solid line, Fig 4H), thus breaking the reciprocity typically observed in pairwise interactions.

To investigate the origin of these deviations (faster motion, deeper swimming, larger separations, and reduced alignment) we quantified turning behavior and acceleration components.

The real fish exhibited much stronger turning dynamics when interacting with the virtual clone. Fig 5A shows the PDF of the signed angular speed $d\phi^+/dt$, defined as the instantaneous heading change signed with the angle of incidence to the wall θ_w, so that left and right turns can be accumulated. The PDF peaks at $d\phi^+/dt \approx 47.5°\ s^{-1}$ in C1, compared with only $\approx 21°\ s^{-1}$ in 2R, and shows a greatly increased probability of extreme turns (high-value tail for $d\phi^+/dt > 100°/s$ in purple line). We also note that the mean time separating a U-turn performed by one fish and that of its companion is higher in C1, 6.6 ± 12.7 s, than in the 2R condition, 3.2 ± 5.1 s (S4 Fig). Since the time intervals between U-turns executed by either the real or the virtual fish's partner are similar, this suggests that the virtual fish's inability to keep up with the real fish stems from its limited acceleration capability.

Kinematic forces are also amplified; the absolute mean parallel acceleration nearly doubles, $\langle |a_{\parallel}| \rangle \approx 5.2\ cm\,s^{-2}$ in C1 vs. $2.5\ cm\,s^{-2}$ in 2R, and the perpendicular acceleration nearly triples: $\langle |a_{\perp}| \rangle \approx 9.9\ cm\,s^{-2}$ in C1 vs. $3.5\ cm\,s^{-2}$ (Figs 5B and 5C).

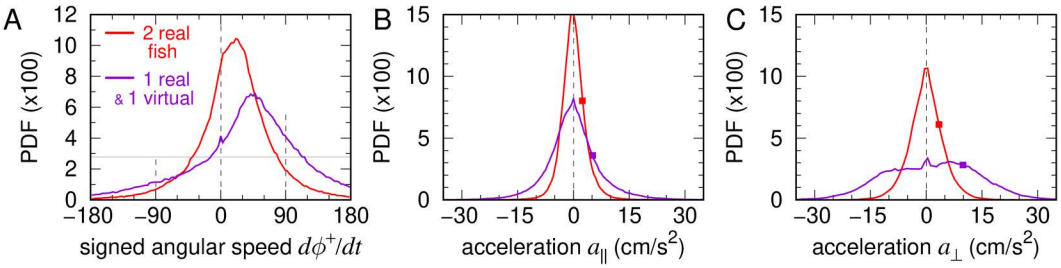

Fig 5. Real–virtual interactions induce stronger turning accelerations. Probability density functions (PDFs) of kinematic variables describing turning maneuvers when the focal fish interacts with a real (red) or a virtual (violet) partner: **(A)** Signed angular velocity $d\phi^+/dt$ (sign defined by the incidence angle θ_w), **(B)** Parallel acceleration $a_{\parallel}$, **(C)** Perpendicular acceleration $a_{\perp}$. Squares in (B, C) indicate the absolute mean accelerations $\langle |a_{\parallel}| \rangle$ and $\langle |a_{\perp}| \rangle$, showing that perpendicular accelerations are more than twice as large as parallel ones when swimming with a virtual partner.

https://doi.org/10.1371/journal.pcbi.1014544.g005

Together, these observations reveal that although the model-controlled virtual fish can elicit coordinated interactions, the lack of full reciprocity and the inability of the virtual fish to match the real fish's acceleration lead to a fundamental disruption of pair cohesion and alignment.

2.4.2 Behavioral response of a real fish to a faster virtual conspecific, with or without reciprocal interactions. In Condition C1, the real fish swam considerably faster than when paired with a real conspecific in the VR setup. This observation motivated us to examine how a real fish responds when the virtual partner swims at that same higher speed, which coincides with the typical real fish speed observed in quasi-2D setups [5]. We refer to this configuration as Condition C2. Furthermore, to test the role of reciprocal interaction, we implemented a third configuration (Condition C3) in which the virtual fish behaves as an isolated agent and does not respond to the real fish. Any coordination in C3 thus arises solely from the real fish adapting to the virtual one.

For each condition, we plotted the PDFs of the relevant behavioral variables: Condition C2 shown in the upper rows of Figs 6–8, and Condition C3 in the bottom rows. We also include numerical simulations in which both agents follow the behavior of the virtual fish. In C3, these simulations represent a "null model" without reciprocal interactions. The parameter values of the model used in these different conditions are provided in S1 Table. The kinematic differences between the virtual fish in conditions C1 and C2 are shown in S5 Fig.

As expected, in both C2 and C3 the real fish swims faster than in 2R, but not substantially faster than in C1. The speed distributions peak at $v_{C2} \approx 7.5$ cm/s (Fig 6A) and $v_{C3} \approx 9$ cm/s (Fig 6D), close to $v_{C1} \approx 8$ cm/s (Fig 4A). However, high-speeds ($v > 15$ cm/s) are more frequent in both C2 and C3 than in C1.

In C2, the virtual fish exhibits nearly identical speed and depth PDFs as the real fish (Figs 6A and 8A), showing that both fish successfully track each other. Their distance to the wall r_w and their wall-incidence angle θ_w converge towards values observed for two real fish (Fig 6B and 6C). These results indicate that the higher speed of the virtual fish enhances mutual responsiveness and improves bidirectional coordination compared with C1.

From the collective perspective, the distance between fish is considerably smaller in C2 (Fig 7A) than in C1 (Fig 4G), and the distribution of heading differences ($\Delta\phi$ and $\Delta\chi$) is much more peaked around zero (Fig 7C), demonstrating higher alignment (see also S2 Video and S2 Fig). This suggests that the speed of the virtual fish modulates the intensity

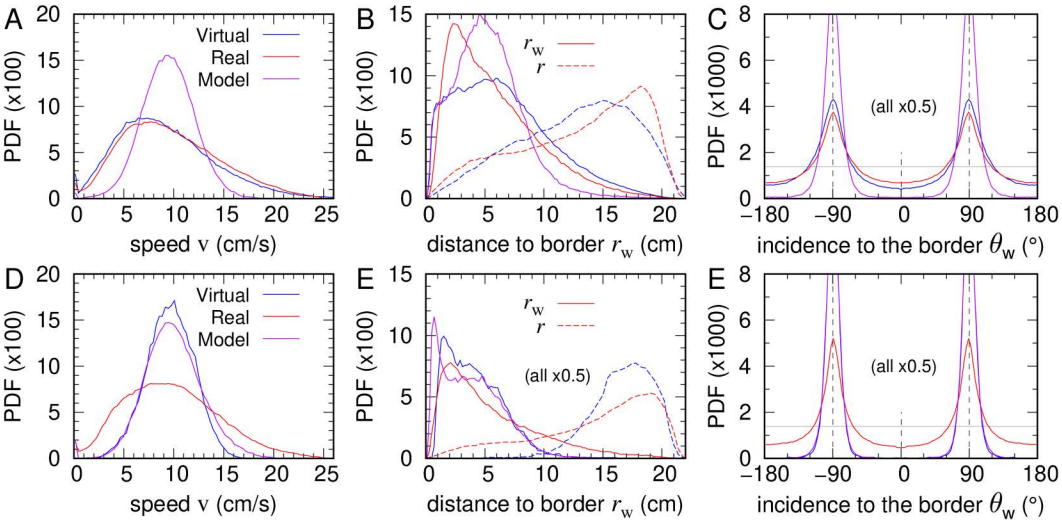

Fig 6. Individual behavioral responses to a faster virtual conspecific with and without social interactions. Probability density functions (PDFs) of real fish (red), the virtual fish (blue), and simulations of the 2R-based model (violet) at a higher mean speed $v \approx 10$ cm/s. **(A–C)** Condition C2: with social interactions enabled (bidirectional coordination). **(D–F)** Condition C3: without social interactions (unilateral interaction). **(A, D)** Swimming speed v. **(B, E)** Distance to the wall r_w. **(C, F)** Incidence angle relative to the wall θ_w.

https://doi.org/10.1371/journal.pcbi.1014544.g006

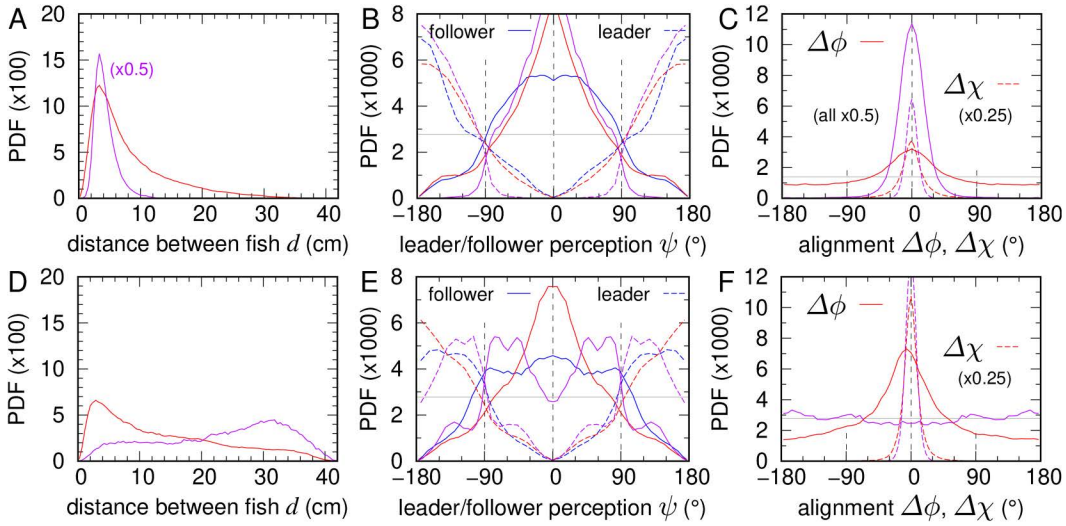

Fig 7. Effects of reciprocal vs. unilateral interaction with a faster virtual partner on collective coordination. Probability density functions (PDFs) of collective variables measured for pairs composed of a real fish (red) and a faster virtual fish (blue), controlled by the 2R-based model, compared with numerical simulations where both agents behave like the virtual one (violet). The mean speed of the virtual fish is increased to v ≈ 10 cm/s. **(A–C)** Condition C2: bidirectional interaction, where the virtual fish responds to the real one. **(D–F)** Condition C3: unilateral interaction, where the virtual fish behaves independently of the real one. **(A, D)** Horizontal inter-individual distance *d*. **(B, E)** Viewing angle ψ for geometrical leader and follower. **(C, F)** Heading alignment between the real and virtual fish in the horizontal plane $\Delta\phi$ and vertical direction $\Delta\chi$.

https://doi.org/10.1371/journal.pcbi.1014544.g007

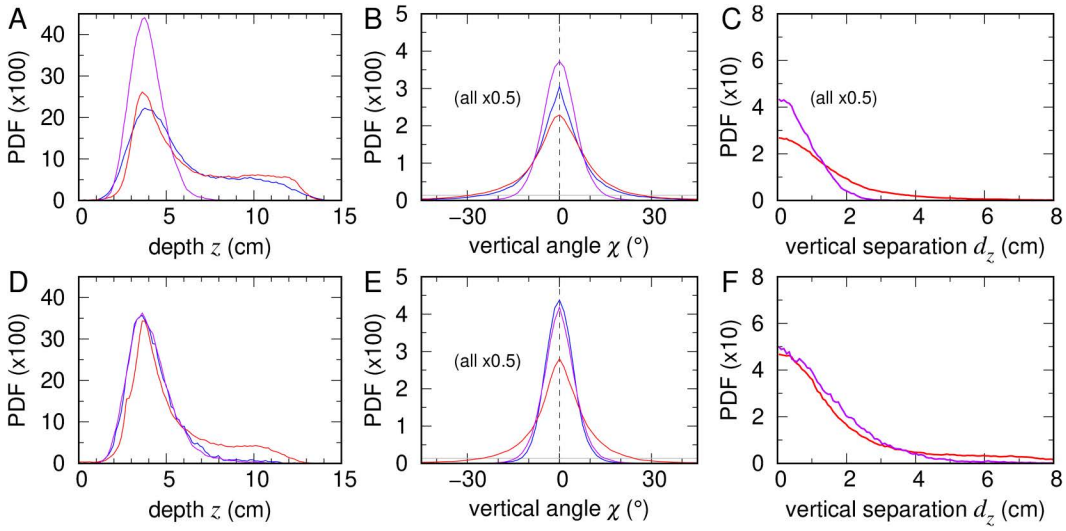

Fig 8. Effects of reciprocal vs. unilateral interaction with a faster virtual partner on vertical motion. Probability density functions (PDFs) of vertical behavioral variables for a real fish (red), a faster virtual fish (blue), and simulations of the 2R-based model (violet), using a higher mean virtual speed v ≈ 10 cm/s. **(A–C)** Condition C2: social interactions enabled (bidirectional coordination). **(D–F)** Condition C3: social interactions disabled (unilateral interaction). **(A, D)** Swimming depth *z*. **(B, E)** Elevation angle χ. **(C, F)** Vertical inter-individual distance d_z.

https://doi.org/10.1371/journal.pcbi.1014544.g008

of alignment interactions. When the virtual fish swims faster, alignment between the two fish is higher. Moreover, the mean time separating a U-turn performed by one fish and that of its companion is smaller in C2 than in C1 (2.4 ± 3.0 s) and close to the 2R condition (S4 Fig).

In sharp contrast, when the virtual fish ignores the real one (Condition C3), the virtual agent behaves exactly as in the null model, but the real fish still reacts socially (see also S3 Video and S1D Fig). As a result, the distance between fish is significantly larger than in C2, yet remains much smaller than expected from the null model in the absence of social interactions (Fig 7D). The alignment between the real and virtual fish, although reduced relative to C1, is still more pronounced than in C2 (Fig 7F), meaning that the alignment between fish is higher when interactions are unidirectional.

Moreover, the unilateral social response in C3 causes the real fish to behave predominantly as a follower, doing so for 57.2% of the time, compared to 38.8% in C1 and 46.6% in C2. In this configuration, the real fish is more frequently positioned behind the virtual partner and follows its trajectory, resulting in similar headings and thus increased alignment ($|\psi| < 90°$; solid red line in Fig 7E). This effect is further reinforced by the low turning rate of the virtual fish in C3, which performs very few U-turns.

To quantify alignment in a single scalar, we computed the average heading difference $\langle \cos \Delta\phi \rangle$ for each condition, obtaining 0.59 for 2R, 0.03 for C1, 0.29 for C2, and 0.35 for C3. These values confirm that the alignment is highest for two real fish, approximately the same in C2 and C3 (although slightly higher in C3), and markedly reduced in C1. We also calculated the U-turn rate of each fish (per 1000 frames), finding 1.8 for 2R, 4.3 (real) and 1.0 (virtual) in C1, 7.7 (real) and 4.8 (virtual) in C2, and 4.5 (real) and 0.4 (virtual) in C3. Due to the high turning rate in C2, for both the real and virtual fish, the alignment is easily disrupted despite that social interactions are in both directions, while in C3, U-turns are practically absent in the trajectory of the virtual fish, making it highly predictable, thus reinforcing the alignment of the follower.

3 Discussion

Understanding how real organisms coordinate their movements requires models that accurately capture the rules they follow [2,37]. A powerful way to validate such models is to directly insert a simulated organism into a natural interaction and observe how a real animal responds [13,14,16,17,23,32]. In this study, we mixed a real fish with its digital twin by using a closed-loop virtual reality system. We first measured and reconstructed the social interaction functions between two real fish swimming freely in a semi-spherical bowl, allowing precise quantification of their three-dimensional trajectories and mutual responses. Then, we developed a 3D behavioral model incorporating these functions and demonstrated that it reproduced natural coordination dynamics. Finally, we embedded this model in an immersive VR setup so that a virtual fish could interact in real time with a real fish. We used these experiments to test whether the model captures the social forces that govern pairwise swimming. This study provides a crucial step toward strong validation of models of collective behavior in living systems.

A first result is that the reconstructed interaction model quantitatively reproduces both individual and collective level dynamics in 3D simulations involving two virtual fish. When the agents are controlled by the interaction functions extracted from real pairs, they exhibit key features of natural swimming behavior: they remain close to the wall, maintain a preferred depth, and sustain an attraction that is strong enough to maintain tight spatial cohesion. Their distributions of speed, angular velocity, and inter-individual positioning closely match experimental baselines involving two real fish. These results are consistent with prior 2D reconstructions of attraction and alignment forces in burst-and-coast swimmers [5,36] and support the general idea that visual cues alone can sustain coordinated motion in social fish [29–31,38]. These results also demonstrate that the 3D self-propelled particle model captures the core geometric and sensory constraints shaping fish interactions, and that data-driven interaction rules can generate realistic collective motion in 3D environments.

When we allowed the virtual fish to interact in real time with a live fish (Condition C1), some differences emerged. The real fish often swam faster and executed sharper turns than in natural pairs, leading to greater separation and reduced alignment. Although the interaction rules were correct and allowed the real and virtual fish to coordinate their swimming when they were close to each other, the virtual partner could not always match the rapid acceleration and tight turning exhibited by a real fish. As a result, mutual responsiveness was weakened and insufficient to fully maintain cohesion. These results reveal a key requirement for model realism, showing that virtual agents must not only follow accurate

perceptual and social rules but also reproduce biomechanical limits and actuation capabilities [39] in order to sustain stable coordination.

The second finding is that swimming speed modulates the strength of social coordination in agreement with a growing body of literature demonstrating that faster individuals exhibit stronger alignment and influence within groups [40,41]. When we increased the preferred speed of the virtual fish (Condition C2), the real fish matched that speed almost exactly. Both individuals successfully tracked each other. Their distance from the wall and their alignment angles became close to those of two real fish. Spatial cohesion improved markedly compared to Condition C1. These results demonstrate that a faster virtual partner improves joint coordination. The real fish intensified its social response when swimming with a faster conspecific. When movement becomes faster, it amplifies the salience of social cues [42] and elicits stronger reciprocal feedback. Similar observations have been made in studies of flocking birds or schooling fish exposed to threats [24,25], where speed elevation leads to stronger alignment and reduced reaction delays. Consistent with these findings, experiments using an extremely social robotic fish have shown that an individual's mean swimming speed strongly influences group cohesion, polarization, and spatial structure [26]. Our closed-loop experiments provide a controlled demonstration that kinematic context can push the system toward more stable collective motion.

A third key result concerns unilateral interactions (Condition C3). Even when the virtual fish no longer responded to the real one, the pair maintained a striking level of coordination. The real fish continued to match the virtual partner's heading and orientation, far beyond what would be expected from a null model lacking social feedback. This relatively high alignment arises from a persistent follower configuration. Because the virtual fish follows a predictable trajectory with limited directional changes, the real fish can maintain alignment by tracking it from behind. The main difference lies in the increased separation distance. Unlike a responsive partner, the virtual agent does not adjust its trajectory to preserve proximity, allowing brief episodes of larger spacing to accumulate over time. As a result, the distance distribution shifts toward higher values, not because coordination breaks down, but because the interaction becomes inherently non-reciprocal. Overall, the strong social persistence exhibited by the real fish highlights the robustness of the underlying behavioral strategy, even when reciprocal feedback is absent. This finding sheds light on interaction asymmetries and leadership dynamics in collective systems [24,27,28,43]. Recent volumetric VR experiments with freely swimming zebrafish further show that coordination involves not only spatial responses but also a robust, out-of-phase temporal alternation of burst events that emerges exclusively when feedback is reciprocal [17]. This temporal coupling enhances an individual's ability to track sudden directional changes in a partner, revealing a complementary mechanism of coordination that sits alongside the spatial and kinematic factors explored in our closed-loop experiments. The comparison highlights that reciprocity governs not only the geometry of coordination but also its fine-scale temporal structure, pointing to a richer interplay between timing, perception, and social responsiveness in fish.

Every experimental system has limitations. The virtual fish cannot match the full biomechanical capabilities of a real one. In particular, the model does not account for hydrodynamic effects that real fish can perceive at close range and use to coordinate their motion through neighbor-induced flows, such as alternating vortex patterns that can be exploited to reduce energetic cost or enhance propulsion [44,45]. The degree to which real fish perceive the projected stimulus as a mate may also vary with context [23]. Moreover, pair interactions represent only the simplest unit of schooling dynamics, while real groups involve multiple neighbors, distributed sensing, and rapid switching of social roles. These constraints likely contributed to reduced alignment in VR conditions.

Although pairs of real fish and real-virtual fish pairs display a strong vertical alignment and limited depth differences, natural schools exhibit fully three-dimensional organization. Recent work using the same closed-loop virtual reality framework shows that fish respond primarily to a single most influential neighbor at any given time, whose identity changes dynamically [35]. This selective interaction mechanism is sufficient to sustain coordinated motion while allowing flexible spatial organization. In larger groups, the continuous switching of influential neighbors introduces variability in depth, leading to a broader three-dimensional distribution of individuals. Despite these constraints, our results demonstrate that

closed-loop interactions in virtual reality can produce highly realistic social responses. This approach offers new opportunities to test mechanisms that are difficult to isolate in group experiments.

Overall, our findings demonstrate that real fish can form coordinated pairs with model-driven virtual conspecifics, confirming that the social interaction functions reconstructed from real pairs reliably reproduce natural collective behavior. Coordination increases with swimming speed and remains robust even when the model is challenged by unilateral feedback. Thus, mixing real and simulated agents is not only feasible but yields biologically meaningful interactions that directly validate the mechanisms encoded in behavioral models. By placing a digital twin into a natural feedback loop, we overcome a common limitation of collective behavior models and move beyond validation based solely on statistical agreement to directly testing behavioral responses [6,46–48]. Our approach tests whether a model elicits the correct actions in the real organism itself, a far stronger and more mechanistic benchmark.

Several future improvements are already tractable. Enhancing the biomechanical realism of the virtual agent and scaling to multi-agent interactions will allow us to test complex hypotheses about perception, the combination of interactions between neighbors, and decision-making in collective behavior. Similar closed-loop VR methods have begun to reveal prediction error signals in zebrafish [15] and speed-dependent modulation of coordination in fish groups [26,38], highlighting the relevance of our approach to sensory and cognitive dynamics.

Beyond its implications for schooling fish, this hybrid architecture offers a versatile platform for hypothesis testing in living systems. By merging data-driven models with interactive VR, we create adaptive, testable digital twins for collective behavior. This development paves the way toward mixed swarms of biological and digital agents, enabling experiments that would be impossible using only real or simulated organisms. Similar hybrid approaches have successfully merged robotic and animal societies [49–51], while interactive VR platforms now allow real-time bidirectional feedback between real and virtual agents [16,23]. Our work therefore represents a critical step toward fully integrative, closed-loop studies of perception, decision-making, and collective intelligence in animal groups [52,53].

4 Materials and methods

4.1 Ethics statement

Experiments were approved by the Animal Experimentation Ethics Committee C2EA-01 of the Toulouse Biology Research Federation and were performed in an approved fish facility (A3155501) under permit APAFIS#27303–2020090219529069 v8 in agreement with the French legislation. All procedures were designed to minimize stress and handling. Fish were transferred from rearing tanks to the experimental setup with minimal manipulation. Each individual was used in only one one-hour experimental session per week. Swimming ability was monitored throughout; fish exhibiting impaired or absent swimming activity were excluded and replaced. No animals were sacrificed during this study.

4.2 Study species

Rummy-nose tetras (*Hemigrammus rhodostomus*) were purchased from Amazonie Labège in Toulouse, France. Fish were kept in 16 L aquariums on a 12:12 hour, dark:light photoperiod, at 27.7° C ($\pm$0.4) and were fed *ad libitum* with fish flakes. The average body length of the fish used in these experiments is 3.1 cm.

4.3 Experimental setup

We used a closed-loop virtual reality system specifically developed to study real-time interactions between freely swimming fish and computer-generated virtual conspecifics. The virtual fish consisted of a realistic three-dimensional animated model of the rummy-nose tetra (*Hemigrammus rhodostomus*), reproducing the species' body shape, coloration, and swimming kinematics. The model includes characteristic visual features such as the red head and striped tail. The virtual fish is rendered in real time using a Unity-based engine and projected onto the inner surface of the hemispherical tank. Crucially,

the projection is computed using an anamorphic transformation that continuously adapts the size, orientation, and position of the image to the tracked position of the real fish. This ensures that the virtual fish appears as a spatially coherent object located within the three-dimensional environment of the tank, rather than as a distorted image on its surface. The rendering pipeline reconstructs, for each pixel of the projection, the direction of the corresponding light ray relative to the fish's viewpoint, effectively simulating the visual scene from its perspective. This approach creates a consistent perceptual illusion of a freely swimming conspecific [23].

The setup consisted of a hemispherical acrylic bowl (diameter 52.2 cm, depth 14.6 cm, filled with 15 L of water) placed above a DLP LED projector that displayed the anamorphically rendered virtual fish onto the bowl wall. Fish movements were tracked from above using an Intel RealSense D435 depth camera positioned 47.9 cm above the water surface. Infrared illumination (8 IR lamps, 850 nm) enabled robust tracking under controlled light conditions. A dedicated workstation (Dell Precision 3640 with NVIDIA RTX 3070) processed all tasks in real time, including 3D tracking, trajectory simulation of virtual fish, and rendering.

The system included three software modules: a Python-based 3D tracking pipeline, a C++ trajectory simulator, and a Unity rendering engine. In this study, the system was used in closed-loop mode: the position and heading of the virtual fish were continuously controlled by the behavioral model parameterized for rummy-nose tetras, exploiting the current position and speed of the real fish. Real and virtual fish positions were exchanged via UDP at 30–90 Hz, ensuring precise, biologically relevant interactions. The same setup was also employed to study the behavior and interactions of pairs of real fish, using the same structured background and identical lighting conditions as in experiments involving one real and one virtual fish.

4.4 Experimental procedure

We conducted four series of experiments combining behavioral recordings of real fish pairs and closed-loop VR assays. In the first series, we tracked pairs of *H. rhodostomus* swimming freely in a confined 3D space to characterize their spontaneous motion and social interactions. Sixteen one-hour replicates were performed. The collected trajectories provided reference values for swimming speed, spatial positioning, and alignment between individuals, and were used to extract analytical functions describing self-propulsion, wall avoidance, and social interaction terms. These functions formed the basis of the behavioral model controlling the virtual fish. In subsequent experiments, a single real fish was introduced into the hemispherical VR tank and exposed to a virtual conspecific whose motion was governed in real time by this model. The position and heading of the virtual fish were continuously updated in closed loop based on the current position and velocity of the real fish. Three experimental conditions were tested, each defined by a distinct set of model parameters (S1 Table). Condition C1 corresponded to the reference parameter set reproducing the dynamics of two real fish swimming together (see S1 Video). Condition C2 used higher self-propulsion parameters to match the increased swimming speed observed in C1 (see S2 Video). Condition C3 used the same parameters as C2 but with all social interaction terms disabled, such that the virtual fish moved independently of the real one (see S1 Video). Eight one-hour replicates were performed under C1 and C3, and twelve under C2. Each trial began after a 10 min acclimation period.

4.5 Preprocessing of fish trajectories

Before analyzing the trajectories extracted from the experiments, the data must be preprocessed to ensure accuracy and to retain only periods in which fish are actively swimming. Time intervals during which a fish remains immobile for at least 4 seconds are discarded, as well as segments in which its instantaneous speed exceeds 25 cm/s or when it swims in a straight line at approximately constant speed for more than one second. These empirical thresholds were determined from the statistical properties of spontaneous swimming behavior and correspond, respectively, to periods of inactivity and to tracking artifacts such as sudden position jumps.

The dataset is then filtered to remove any frames in which the reconstructed position lies outside the bowl. To recover continuous temporal trajectories, gaps created during this filtering procedure are linearly interpolated whenever the duration of missing data is shorter than one second. For longer gaps, reliable reconstruction is not possible, and the trajectory is left discontinuous at that point.

The resulting trajectories therefore consist of multiple consecutive temporal segments. Each segment is subsequently smoothed by a Gaussian kernel convolution in order to reduce tracking noise while preserving the essential kinematic features of the motion,

$$x(n\Delta t) = \frac{\sum_{i=-n}^{n} x[(n+i)\Delta t] \exp\left(-\left(\frac{i\Delta t}{h}\right)^2\right)}{\sum_{i=-n}^{n} \exp\left(-\left(\frac{i\Delta t}{h}\right)^2\right)}, \tag{9}$$

where $n = 4h/\Delta t$, such that the exponential kernel weight is negligible at $i = n$. The kernel width is set to $h = 0.5$ s (**which is the typical** duration of a kick arising from the burst-and-coast swimming mode of *H. rhodostomus*), which provides minimal smoothing while reducing high-frequency noise.

4.6 Quantification of individual and collective behavior in pair of fish

Fish predominantly swim in the horizontal plane at a preferred comfort depth. Throughout the manuscript, three-dimensional quantities are denoted with a superscript 3D, horizontal (2D) quantities without a superscript, and vertical components with a subscript z.

The experimental bowl is modeled as the lower cap of a sphere of radius $R_0 = 26.19$ cm, filled with 15 liters of water, resulting in a central depth of $h_{\text{water}} = 14.73$ cm. The coordinate origin is placed at the water surface above the center of the bowl, with the z-axis oriented downward so that depth values are positive and increase with distance from the surface. At depth z, the radius of the corresponding horizontal cross-section is

$$R_z = \sqrt{R_0^2 - (R_0 - h_{\text{water}} + z)^2}, \tag{10}$$

which vanishes at $z = h_{\text{water}}$, as expected.

The fish position and velocity are given by the vectors $\vec{u}^{\,3D} = (x, y, z)$ and $\vec{v}^{\,3D} = (v_x, v_y, v_z)$. We define the distance to the bowl's vertical axis as $r = \|(x, y)\|$ and the distance to the horizontal boundary at depth z as $r_w = R_z - r$. For consistency with previous work, we refer to this horizontal boundary as the *wall*.

The horizontal velocity is $\vec{v} = (v_x, v_y)$, and the full 3D speed and its horizontal component are $v^{3D} = \|\vec{v}^{\,3D}\|$ and $v = \|(v_x, v_y)\|$, respectively. The fish heading in the horizontal plane is defined as $\phi = \text{atan2}(v_y, v_x)$, ranging from $-\pi$ to π, while the elevation angle is $\chi = \text{atan}(v_z/v)$, ranging in $(-\pi/2, \pi/2)$ when $v > 0$. Heading is used to compute the angle of incidence to the wall, $\theta_w = \phi - \theta$, where $\theta = \text{atan2}(y, x)$ is the positional azimuth. By convention, positive headings are counterclockwise, and positive (negative) elevation indicates upward (downward) motion.

When swimming with a conspecific, the relative configuration is defined by their spatial separation and angular alignment. For a pair of fish i and j, the 3D distance between them is $d_{ij}^{3D} = \|\vec{u}_i^{\,3D} - \vec{u}_j^{\,3D}\|$, the horizontal distance $d_{ij} = \|(x_i, y_i) - (x_j, y_j)\|$, and the vertical distance $d_{ij}^z = |z_i - z_j|$. The *viewing angle* ψ_{ij}, defined as the angle fish i has to turn to point toward fish j, is computed as $\psi_{ij} = \text{atan2}(y_j - y_i, x_j - x_i) - \phi_i$. Note that, in general, $\psi_{ij} \neq -\psi_{ji}$, meaning interaction geometry is not necessarily reciprocal.

We define the *geometrical leader* as the individual with the larger perception angle magnitude $|\psi_{ij}|$, while the other fish is considered the *geometrical follower*. Alignment differences in the horizontal and vertical planes are given by $\phi_{ij} = \phi_j - \phi_i = -\phi_{ji}$ and $\chi_{ij} = \chi_j - \chi_i = -\chi_{ji}$.

Since only dyads are studied here, notation is simplified by omitting indices when no ambiguity arises, writing $d, \psi, \Delta\phi, \Delta\chi$ instead of $d_{ij}, \psi_{ij}, \phi_{ij}, \chi_{ij}$.

4.7 3D self-propelled particle model for fish swimming in a bowl

The horizontal velocity of a fish is decomposed into components parallel and perpendicular to its instantaneous heading. Defining the unit vectors

$$\vec{e}_{\parallel} = (\cos\phi, \sin\phi), \quad \vec{e}_{\perp} = (-\sin\phi, \cos\phi),$$

the velocity in the horizontal plane is $\vec{v} = \mathrm{v}\,\vec{e}_{\parallel}$. The horizontal acceleration is written as $\vec{a} = a_{\parallel}\vec{e}_{\parallel} + a_{\perp}\vec{e}_{\perp}$, where $a_{\parallel}$ and $a_{\perp}$ are the longitudinal (speed-changing) and lateral (turning) acceleration components, respectively. Together with the vertical acceleration a_z, these variables fully determine the temporal evolution of fish position.

Expressing each force as the product of a scalar with the unit vector of its direction, the components of fish's acceleration in the horizontal plane are as follows:

$$\begin{aligned}\frac{d\vec{v}_i(t)}{dt} = &-\left[F_{\text{water}}(\vec{v}_i) + F_{\text{adapt}}(\vec{v}_i)\right]\vec{e}^{\,i}_{\parallel}(t) + \vec{\eta}(t) - F_{\text{w}}(r^i_{\text{w}}, \theta^i_{\text{w}})\vec{e}_i(t) + F_{\text{rot}}(r^i_{\text{w}}, \theta^i_{\text{w}})\vec{e}^{\,i}_{\perp}(t)\\ &+ F_{\text{Att}}(d_{ij}, \psi_{ij}, \phi_{ij})\vec{e}_{ij}(t) + F_{\text{Ali}}(d_{ij}, \psi_{ij}, \phi_{ij})\vec{e}^{\,i}_{\perp}(t),\end{aligned} \tag{11}$$

where $\vec{e}_i = (\cos\theta_i, \sin\theta_i)$, with $\theta_i = \text{atan2}(y_i, x_i)$, is the position angle of fish i in the horizontal plane and is perpendicular to the wall closest to the fish in the horizontal plane, and $\vec{e}_{ij} = (\cos\theta_{ij}, \sin\theta_{ij})$, with $\theta_{ij} = \text{atan2}(y_j - y_i, x_j - x_i)$, is oriented along the direction from i to j in the horizontal plane.

Using $\psi_{ij} = \theta_{ij} - \phi_i$ and $\theta^i_{\text{w}} = \phi_i - \theta_i$, the vectors $\vec{e}_i$ and $\vec{e}_{ij}$ can be expressed in the fish frame as $\vec{e}_{ij} = \cos\psi_{ij}\,\vec{e}_{\parallel} + \sin\psi_{ij}\,\vec{e}_{\perp}$ and $\vec{e}_i = \cos\theta^i_{\text{w}}\,\vec{e}_{\parallel} - \sin\theta^i_{\text{w}}\,\vec{e}_{\perp}$.

In the intrinsic frame of fish i, this gives the scalar components of the acceleration:

$$a^i_{\parallel} = -\left[F_{\text{water}}(\vec{v}_i) + F_{\text{adapt}}(\vec{v}_i)\right] - F_{\text{w}}(r^i_{\text{w}}, \theta^i_{\text{w}})\cos\theta^i_{\text{w}} + F_{\text{Att}}(d_{ij}, \psi_{ij}, \phi_{ij})\cos\psi_{ij} + \eta_{\parallel}, \tag{12}$$

$$a^i_{\perp} = F_{\text{w}}(r^i_{\text{w}}, \theta^i_{\text{w}})\sin\theta^i_{\text{w}} + F_{\text{rot}}(r^i_{\text{w}}, \theta^i_{\text{w}}) + F_{\text{Att}}(d_{ij}, \psi_{ij}, \phi_{ij})\sin\psi_{ij} + F_{\text{Ali}}(d_{ij}, \psi_{ij}, \phi_{ij}) + \eta_{\perp}. \tag{13}$$

Using explicitly the decomposition of the interactions into products of single-variable functions, the final system reads

$$\begin{aligned}a^i_{\parallel} = &-\left[f_{\text{water}}(\mathrm{v}_i) + f_{\text{adapt}}(\mathrm{v}_i - \bar{\mathrm{v}}_i)\right] - f_{\text{w}}(r^i_{\text{w}})\,g_{\text{w}}(\theta^i_{\text{w}})\cos\theta^i_{\text{w}}\\ &+ f_{\text{Att}}(d_{ij})\,g_{\text{Att}}(\psi_{ij})\,h_{\text{Att}}(\phi_{ij})\cos\psi_{ij} + \eta_{\parallel},\end{aligned} \tag{14}$$

$$\begin{aligned}a^i_{\perp} = &\, f_{\text{w}}(r^i_{\text{w}})\,g_{\text{w}}(\theta^i_{\text{w}})\sin\theta^i_{\text{w}} + f_{\text{rot}}(r^i_{\text{w}})\,g_{\text{rot}}(\theta^i_{\text{w}})\sin\theta^i_{\text{w}}\\ &+ f_{\text{Att}}(d_{ij})\,g_{\text{Att}}(\psi_{ij})\,h_{\text{Att}}(\phi_{ij})\sin\psi_{ij} + f_{\text{Ali}}(d_{ij})\,g_{\text{Ali}}(\psi_{ij})\,h_{\text{Ali}}(\phi_{ij})\sin\phi_{ij} + \eta_{\perp},\end{aligned} \tag{15}$$

$$a^i_z = -f^z_{\text{water}}(\mathrm{v}^i_z) - f^z_{\text{comfort}}(z_i) + f^z_{\text{Att}}(d_{ij})\,k^z_{\text{Att}}(d^z_{ij})\,g^z_{\text{Att}}(\psi_{ij})\,h^z_{\text{Att}}(\phi_{ij}) + \eta_z, \tag{16}$$

where $\bar{\mathrm{v}}_i = \left(\sum_{j=1, j\neq i}^{N} \mathrm{v}_j\right)/(N-1)$ is the average speed of the neighbor(s) of i, which for $N=2$ fish becomes $\bar{\mathrm{v}}_i = \mathrm{v}_{3-i}$, $i=1,2$.

The analytical expressions of the different functions arising in these equations of motion (5 polynomial expansions, 8 Fourier series, and 5 simple fits of tabulated functions), used in the reconstruction procedure and implemented in the model, are given in Supplemental Material.

4.7.1 Stochasticity. Behavioral fluctuations are modeled as autocorrelated noise processes in the parallel, perpendicular, and vertical directions. Noise components are defined in the fish-centered reference frame and converted into Cartesian coordinates via

$$\eta_x = \eta_{\parallel}\cos\phi - \eta_{\perp}\sin\phi, \quad \eta_y = \eta_{\parallel}\sin\phi + \eta_{\perp}\cos\phi.$$

They evolve according to a discrete Ornstein-Uhlenbeck process with time-step index n,

$$\eta_{\parallel}^{n+1} = a\,\eta_{\parallel}^{n} + b_{\parallel}g_{\parallel}, \quad \eta_{\perp}^{n+1} = a\,\eta_{\perp}^{n} + b_{\perp}g_{\perp}, \quad \eta_z^{n+1} = a_z\eta_z^{n} + b_z g_z,$$

where $g_{\parallel}$, $g_{\perp}$, g_z are independent random numbers normally distributed, generated with the Box-Muller transform: $g = \sqrt{-2\ln(u_1)}\cos(2\pi u_2)$, $u_1, u_2 \sim \mathcal{U}(0,1)$. The parameters corresponding to the Ornstein-Uhlenbeck dynamics are given by

$$a = e^{-\Delta t/\tau}, \quad b_{\parallel} = \sigma_{\parallel}\sqrt{1-e^{-2\Delta t/\tau}}, \quad b_{\perp} = \sigma_{\perp}\sqrt{1-e^{-2\Delta t/\tau}}, \quad a_z = e^{-\Delta t/\tau_z}, \quad b_z = \sigma_z\sqrt{1-e^{-2\Delta t/\tau_z}},$$

where $\sigma_{\parallel}$, $\sigma_{\perp}$, and σ_z set noise amplitudes, and τ, τ_z are correlation times in the horizontal and vertical directions, respectively, that we took equal in practice. The occurrence of finite correlation times for the noises is consistent with the true burst-and-coast nature of the fish swimming mode, where a fish alternates a very brief acceleration period (of typical duration 0.1 s) with a passive gliding period lasting typically 0.5 s, where the fish barely changes its heading.

4.7.2 Boundary rejection rules. In this agent-based model, (x,y,z) denotes the center of mass of the fish. Since fish have a finite body length, the predicted position at step $n+1$ may place the head outside the water volume. Such moves are rejected.

The position of the head is obtained from $x_h = x + l_h\cos\phi\cos\chi$, $y_h = y + l_h\sin\phi\cos\chi$, and $z_h = z + l_h\sin\chi$, where l_h is the head-center distance.

Two rejection cases are implemented:

- Collision with the wall: If the head lies beyond the wall surface, $r_w(x_h^{n+1}, y_h^{n+1}, z_h^{n+1}) < 0$, the previous position (x^n, y^n, z^n) is restored, and the fish is reoriented to swim nearly tangentially to the wall (adding a small random angle of order $B \approx 0.15$ radian):

$$\phi^{n+1} = \theta^{n+1} + \mathrm{sign}(\theta_w^n)\,\frac{\pi}{2}(1 + B\,u), \tag{17}$$

$$\eta_{\perp}^{n+1} = \mathrm{sign}(\theta_w^n)\,|\eta_{\perp}^{n+1}|, \tag{18}$$

  where $u \sim \mathcal{U}(0,1)$. This ensures $\theta_w^{n+1} \approx \pm\pi/2$, i.e., near alignment with the wall.

- Exiting the water surface: In the very rarely observed cases where the head is predicted to lie above the surface or below the bowl bottom, the depth is restored and the vertical speed is reversed: $z^{n+1} = z^n$ and $v_z^{n+1} = -v_z^n$.

Supporting information

S1 Fig Comparison of three-dimensional speed and distance between fish with their projections on the horizontal plane. (**A**) Probability density functions (PDF) of the 3D-speed (red) and of its projection on the horizontal plane (violet). (**B**) PDFs of the 3D-distance between fish (red) and of its projection on the horizontal plane (violet).
(PDF)

S2 Fig Real and virtual fish trajectories. (**2R**) Four representative trajectories of a pair of *Hemigrammus rhodostomus* swimming freely in a hemispherical bowl for one minute. (**C1**) Four representative trajectories of a real fish (red) and a virtual fish (blue) that reproduces the behavior of a real fish swimming in a pair for one minute in Condition C1 ($v \approx 5\,cm\,s^{-1}$). (**C2**) Same as C1 but with the virtual fish moving at twice the natural speed ($v \approx 10\,cm\,s^{-1}$) and with reciprocal interactions. (**C3**) Same as C2 but without reciprocal interactions.
(PDF)

S3 Fig Time interval between U-turns. (**A**) Probability density function (PDF) of the time interval between two consecutive U-turns (angle change >100° in 0.5 s) performed by the same fish, measured in experiments with two real fish (red), and in numerical simulations of the model with parameters corresponding to Conditions C1 (dark blue) and C2 (light blue). (**B**) Corresponding survival curves. Straight lines indicate exponential fits.
(PDF)

S4 Fig Time interval between a U-turn of the focal fish and the U-turn of its neighbor. (**A**) Probability density function (PDF) of the time interval between between a U-turn of the focal fish and the U-turn of its neighbor (angle change >100° in 0.5 s), measured in experiments with two real fish (red), and in Conditions C1 and C2. (**B**) Corresponding survival curves.
(PDF)

S5 Fig Kinematics of the virtual fish in conditions C1 and C2. Probability density function (PDF) of (**A**) speed, (**B**) parallel acceleration, and (**C**) perpendicular acceleration.
(PDF)

S1 Table. Values of model parameters used in conditions C1, C2 and C3.
(PDF)

S1 Text. Analytical expressions of the extracted social interaction functions.
(PDF)

S1 Video. Behavioral responses of a real fish interacting with a realistic virtual partner. Video excerpt of an experiment in Condition C1 with a real fish interacting with the anamorphic projection of a virtual conspecific whose motion and interactions with the real fish are controlled in real time by the model. In this condition, the virtual fish is a perfect clone, reproducing the behavior of a real fish in a pair with a mean speed $v \approx 5\,cm\,s^{-1}$. Top-Left: user interface allowing the real-time visualization of the trajectories of the real and virtual fish (in the *xy*-and *xz*-planes) and the instantaneous modification of the parameters of the model driving the virtual fish. Bottom-Left: real-time 3D tracking of the real fish. Right panel: anamorphic rendering of the virtual fish projected onto the bowl by the rendering application according to the 3D position of the real fish.
(MP4)

S2 Video. Behavioral response of a real fish to a faster virtual conspecific with reciprocal interactions. Video excerpt of an experiment in Condition C2 with a real fish interacting with the anamorphic projection of a virtual conspecific whose motion and interactions with the real fish are controlled in real time by the model. In this condition, the virtual fish is moving at twice the natural speed observed for real fish in condition C1 ($v \approx 10\,cm\,s^{-1}$). Top-Left: user interface allowing the real-time visualization of the trajectories of the real and virtual fish (in the *xy*- and *xz*-planes) and the instantaneous modification of the parameters of the model driving the virtual fish. Bottom-Left: real-time 3D tracking of the real fish. Right panel: anamorphic rendering of the virtual fish projected onto the bowl by the rendering application according to the 3D position of the real fish.
(MP4)

S3 Video. Behavioral response of a real fish to a faster virtual conspecific without reciprocal interactions. Video excerpt of an experiment in Condition C3 with a real fish interacting with the anamorphic projection of a virtual conspecific. In this condition, the virtual fish behaves as an isolated agent, moving at a speed of approximately $v \approx 10$ cm s^{-1} according to the model's dynamics, and does not respond to the real fish. Top-Left: user interface allowing the real-time visualization of the trajectories of the real and virtual fish (in the *xy*- and *xz*-planes) and the instantaneous modification of the parameters of the model driving the virtual fish. Bottom-Left: real-time 3D tracking of the real fish. Right panel: anamorphic rendering of the virtual fish projected onto the bowl by the rendering application according to the 3D position of the real fish.
(MP4)

Author contributions

Conceptualization: Stéphane Sanchez, Clément Sire, Guy Theraulaz.

Data curation: Ramón Escobedo.

Formal analysis: Ramón Escobedo, Clément Sire.

Funding acquisition: Stéphane Sanchez, Clément Sire, Guy Theraulaz.

Investigation: Ramón Escobedo, Justine Reynaud, Guy Theraulaz.

Methodology: Clément Sire, Guy Theraulaz.

Project administration: Guy Theraulaz.

Resources: Renaud Bastien, Stéphane Sanchez.

Supervision: Clément Sire, Guy Theraulaz.

Validation: Ramón Escobedo, Clément Sire, Guy Theraulaz.

Visualization: Ramón Escobedo, Stéphane Sanchez.

Writing – original draft: Ramón Escobedo, Clément Sire, Guy Theraulaz.

Writing – review & editing: Ramón Escobedo, Clément Sire, Guy Theraulaz.

References

1. Vicsek T, Zafeiris A. Collective motion. Phys Rep. 2012;517(3–4):71–140. https://doi.org/10.1016/j.physrep.2012.03.004
2. Lopez U, Gautrais J, Couzin ID, Theraulaz G. From behavioural analyses to models of collective motion in fish schools. Interface Focus. 2012;2(6):693–707. https://doi.org/10.1098/rsfs.2012.0033 PMID: 24312723
3. Herbert-Read JE. Understanding how animal groups achieve coordinated movement. J Exp Biol. 2016;219(Pt 19):2971–83. https://doi.org/10.1242/jeb.129411 PMID: 27707862
4. Ouellette NT. A physics perspective on collective animal behavior. Phys Biol. 2022;19(2):10.1088/1478-3975/ac4bef. https://doi.org/10.1088/1478-3975/ac4bef PMID: 35038691
5. Calovi DS, Litchinko A, Lecheval V, Lopez U, Pérez Escudero A, Chaté H, et al. Disentangling and modeling interactions in fish with burst-and-coast swimming reveal distinct alignment and attraction behaviors. PLoS Comput Biol. 2018;14(1):e1005933. https://doi.org/10.1371/journal.pcbi.1005933 PMID: 29324853
6. Lei L, Escobedo R, Sire C, Theraulaz G. Computational and robotic modeling reveal parsimonious combinations of interactions between individuals in schooling fish. PLoS Comput Biol. 2020;16(3):e1007194. https://doi.org/10.1371/journal.pcbi.1007194 PMID: 32176680
7. Xue T, Li X, Lin G, Escobedo R, Han Z, Chen X, et al. Tuning social interactions' strength drives collective response to light intensity in schooling fish. PLoS Comput Biol. 2023;19(11):e1011636. https://doi.org/10.1371/journal.pcbi.1011636 PMID: 37976299
8. Dolins FL, Schweller K, Milne S. Technology advancing the study of animal cognition: using virtual reality to present virtually simulated environments to investigate nonhuman primate spatial cognition. Curr Zool. 2017;63(1):97–108. https://doi.org/10.1093/cz/zow121 PMID: 29491967
9. Judák L, Dobos G, Ócsai K, Báthory E, Szebik H, Tarján B, et al. Moculus: an immersive virtual reality system for mice incorporating stereo vision. Nat Methods. 2025;22(2):386–98. https://doi.org/10.1038/s41592-024-02554-6 PMID: 39668210

10. Isaacson M, Chang H, Berkowitz L, Zirkel R, Park Y, Hu D, et al. MouseGoggles: an immersive virtual reality headset for mouse neuroscience and behavior. Nat Methods. 2025;22(2):380–5. https://doi.org/10.1038/s41592-024-02540-y PMID: 39668209
11. Jouary A, Haudrechy M, Candelier R, Sumbre G. A 2D virtual reality system for visual goal-driven navigation in zebrafish larvae. Sci Rep. 2016;6:34015. https://doi.org/10.1038/srep34015 PMID: 27659496
12. Stowers JR, Hofbauer M, Bastien R, Griessner J, Higgins P, Farooqui S, et al. Virtual reality for freely moving animals. Nat Methods. 2017;14(10):995–1002. https://doi.org/10.1038/nmeth.4399 PMID: 28825703
13. Naik H, Bastien R, Navab N, Couzin ID. Animals in Virtual Environments. IEEE Trans Vis Comput Graph. 2020;26(5):2073–83. https://doi.org/10.1109/TVCG.2020.2973063 PMID: 32070970
14. Huang K-H, Rupprecht P, Frank T, Kawakami K, Bouwmeester T, Friedrich RW. A virtual reality system to analyze neural activity and behavior in adult zebrafish. Nat Methods. 2020;17(3):343–51. https://doi.org/10.1038/s41592-020-0759-2 PMID: 32123394
15. Torigoe M, Islam T, Kakinuma H, Fung CCA, Isomura T, Shimazaki H, et al. Zebrafish capable of generating future state prediction error show improved active avoidance behavior in virtual reality. Nat Commun. 2021;12(1):5712. https://doi.org/10.1038/s41467-021-26010-7 PMID: 34588436
16. Li L, Nagy M, Amichay G, Wu R, Wang W, Deussen O, et al. Reverse engineering the control law for schooling in zebrafish using virtual reality. Sci Robot. 2025;10(101):eadq6784. https://doi.org/10.1126/scirobotics.adq6784 PMID: 40305578
17. Amichay G, et al. Revealing the mechanism and function underlying pairwise temporal coupling in collective motion. Nat Commun. 2024;15(1):48458. https://doi.org/10.1038/s41467-024-48458-z
18. McKee A, Soto AP, Chen P, McHenry MJ. The sensory basis of schooling by intermittent swimming in the rummy-nose tetra (Hemigrammus rhodostomus). Proc Biol Sci. 2020;287(1937):20200568. https://doi.org/10.1098/rspb.2020.0568 PMID: 33109007
19. Lafoux B, Moscatelli J, Godoy-Diana R, Thiria B. Illuminance-tuned collective motion in fish. Commun Biol. 2023;6(1):585. https://doi.org/10.1038/s42003-023-04861-8 PMID: 37258699
20. Lin G, Escobedo R, Li X, Xue T, Han Z, Sire C, et al. Experimental Evidence of Stress-Induced Critical State in Schooling Fish. PRX Life. 2025;3(3). https://doi.org/10.1103/nr7p-m4ff
21. Lecheval V, Jiang L, Tichit P, Sire C, Hemelrijk CK, Theraulaz G. Social conformity and propagation of information in collective U-turns of fish schools. Proc Biol Sci. 2018;285(1877):20180251. https://doi.org/10.1098/rspb.2018.0251 PMID: 29695447
22. Escobedo R, Lecheval V, Papaspyros V, Bonnet F, Mondada F, Sire C, et al. A data-driven method for reconstructing and modelling social interactions in moving animal groups. Philos Trans R Soc Lond B Biol Sci. 2020;375(1807):20190380. https://doi.org/10.1098/rstb.2019.0380 PMID: 32713309
23. Sanchez S, Escobedo R, Bastien R, Lenseigne B, Denis A, Moreau M, et al. An open-source closed-loop Virtual Reality system to investigate social interactions and collective behavior in fish. PLoS One. 2026;21(1):e0339909. https://doi.org/10.1371/journal.pone.0339909 PMID: 41563960
24. Herbert-Read JE, Buhl J, Hu F, Ward AJW, Sumpter DJT. Initiation and spread of escape waves within animal groups. R Soc Open Sci. 2015;2(4):140355. https://doi.org/10.1098/rsos.140355 PMID: 26064630
25. Attanasi A, Cavagna A, Del Castello L, Giardina I, Grigera TS, Jelić A, et al. Information transfer and behavioural inertia in starling flocks. Nat Phys. 2014;10(9):615–98. https://doi.org/10.1038/nphys3035 PMID: 25264452
26. Jolles JW, Weimar N, Landgraf T, Romanczuk P, Krause J, Bierbach D. Group-level patterns emerge from individual speed as revealed by an extremely social robotic fish. Biol Lett. 2020;16(9):20200436. https://doi.org/10.1098/rsbl.2020.0436 PMID: 32933404
27. Couzin ID, Krause J, Franks NR, Levin SA. Effective leadership and decision-making in animal groups on the move. Nature. 2005;433(7025):513–6. https://doi.org/10.1038/nature03236 PMID: 15690039
28. Herbert-Read JE, Krause S, Morrell LJ, Schaerf TM, Krause J, Ward AJW. The role of individuality in collective group movement. Proc Biol Sci. 2012;280(1752):20122564. https://doi.org/10.1098/rspb.2012.2564 PMID: 23222452
29. Partridge BL, Pitcher TJ. The sensory basis of fish schools: Relative roles of lateral line and vision. J Comp Physiol. 1980;135(4):315–25. https://doi.org/10.1007/bf00657647
30. Lemasson BH, Anderson JJ, Goodwin RA. Collective motion in animal groups from a neurobiological perspective: the adaptive role of visual feedback. J Theor Biol. 2009;261:501–10. https://doi.org/10.1016/j.jtbi.2009.08.015
31. Qin M, Wong A, Seguin D, Gerlai R. Induction of social behavior in zebrafish: live versus computer animated fish as stimuli. Zebrafish. 2014;11(3):185–97. https://doi.org/10.1089/zeb.2013.0969 PMID: 24575942
32. Vidal M, Mills SC, Gairin E, Bertucci F, Lecchini D. Validation of a novel immersive virtual reality set-up with responses of wild-caught freely moving coral reef fish. Anim Behav. 2023;206:99–123. https://doi.org/10.1016/j.anbehav.2023.09.013
33. Liu D, Burbano D. Collective intermittent exploration in fish schools is mediated by visual cues. R Soc Open Sci. 2025;12(6):250033. https://doi.org/10.1098/rsos.250033 PMID: 40568549
34. Larsch J, Baier H. Biological Motion as an Innate Perceptual Mechanism Driving Social Affiliation. Curr Biol. 2018;28(22):3523-3532.e4. https://doi.org/10.1016/j.cub.2018.09.014 PMID: 30393036
35. Kang Z, Escobedo R, Sanchez S, Sire C, Theraulaz G. Decoding social integration in schooling fish using closed-loop real–virtual interactions. bioRxiv. 2026. https://doi.org/10.64898/2026.03.12.711426

36. Wang W, Escobedo R, Sanchez S, Sire C, Han Z, Theraulaz G. The impact of individual perceptual and cognitive factors on collective states in a data-driven fish school model. PLoS Comput Biol. 2022;18(3):e1009437. https://doi.org/10.1371/journal.pcbi.1009437 PMID: 35235565
37. Giardina I. Collective behavior in animal groups: theoretical models and empirical studies. HFSP J. 2008;2(4):205–19. https://doi.org/10.2976/1.2961038 PMID: 19404431
38. Schaerf TM, Dillingham PW, Ward AJW. The effects of external cues on individual and collective behavior of shoaling fish. Sci Adv. 2017;3(6):e1603201. https://doi.org/10.1126/sciadv.1603201 PMID: 28691088
39. Papaspyros V, Theraulaz G, Sire C, Mondada F. Quantifying the biomimicry gap in biohybrid robot-fish pairs. Bioinspir Biomim. 2024;19(4):046020. https://doi.org/10.1088/1748-3190/ad577a PMID: 38866031
40. Katz Y, Tunstrøm K, Ioannou CC, Huepe C, Couzin ID. Inferring the structure and dynamics of interactions in schooling fish. Proc Natl Acad Sci U S A. 2011;108(46):18720–5. https://doi.org/10.1073/pnas.1107583108 PMID: 21795604
41. Puy A, Gimeno E, Torrents J, Bartashevich P, Miguel MC, Pastor-Satorras R, et al. Selective social interactions and speed-induced leadership in schooling fish. Proc Natl Acad Sci U S A. 2024;121(18):e2309733121. https://doi.org/10.1073/pnas.2309733121 PMID: 38662546
42. Pritchard VL, Lawrence J, Butlin RK, Krause J. Shoal choice in zebrafish, Danio rerio: the influence of shoal size and activity. Anim Behav. 2001;62(6):1085–8. https://doi.org/10.1006/anbe.2001.1858
43. Jolles JW, Boogert NJ, Sridhar VH, Couzin ID, Manica A. Consistent Individual Differences Drive Collective Behavior and Group Functioning of Schooling Fish. Curr Biol. 2017;27(18):2862-2868.e7. https://doi.org/10.1016/j.cub.2017.08.004 PMID: 28889975
44. Liao JC. A review of fish swimming mechanics and behaviour in altered flows. Philos Trans R Soc Lond B Biol Sci. 2007;362(1487):1973–93. https://doi.org/10.1098/rstb.2007.2082 PMID: 17472925
45. Li L, Nagy M, Graving JM, Bak-Coleman J, Xie G, Couzin ID. Vortex phase matching as a strategy for schooling in robots and in fish. Nat Commun. 2020;11(1):5408. https://doi.org/10.1038/s41467-020-19086-0 PMID: 33106484
46. Camazine S, Deneubourg JL, Franks NR, Sneyd J, Theraulaz G, Bonabeau E. Self-organization in Biological Systems. Princeton (NJ): Princeton University Press; 2001.
47. Sumpter DJT. Collective Animal Behavior. Princeton (NJ): Princeton University Press; 2010.
48. Weitz S, Blanco S, Fournier R, Gautrais J, Jost C, Theraulaz G. Modeling collective animal behavior with a cognitive perspective: a methodological framework. PLoS One. 2012;7(6):e38588. https://doi.org/10.1371/journal.pone.0038588 PMID: 22761685
49. Halloy J, Sempo G, Caprari G, Rivault C, Asadpour M, Tâche F, et al. Social integration of robots into groups of cockroaches to control self-organized choices. Science. 2007;318(5853):1155–8. https://doi.org/10.1126/science.1144259 PMID: 18006751
50. Faria JJ, Dyer JRG, Clément RO, Couzin ID, Holt N, Ward AJW, et al. A novel method for investigating the collective behaviour of fish: introducing 'Robofish'. Behav Ecol Sociobiol. 2010;64(8):1211–8. https://doi.org/10.1007/s00265-010-0988-y
51. Bonnet F, Kienitz M, Halloy J, Mondada F, Siegwart R. Mixed societies of robots and animals: an integrative approach to study collective behavior. Front Robot AI. 2019;6:75. https://doi.org/10.3389/frobt.2019.00075
52. Krause J, Winfield AFT, Deneubourg J-L. Interactive robots in experimental biology. Trends Ecol Evol. 2011;26(7):369–75. https://doi.org/10.1016/j.tree.2011.03.015 PMID: 21496942
53. Romano D, Donati E, Benelli G, Stefanini C. A review on animal-robot interaction: from bio-hybrid organisms to mixed societies. Biol Cybern. 2019;113(3):201–25. https://doi.org/10.1007/s00422-018-0787-5 PMID: 30430234